



# A Review of the Source Characteristics and Physical Mechanisms of Very Long Period (VLP) Seismic Signals at Active Volcanoes

K. I. Konstantinou<sup>1</sup> 

Received: 15 February 2023 / Accepted: 7 July 2023 / Published online: 5 September 2023  
© The Author(s) 2023

## Abstract

Very Long Period (VLP) signals with periods longer than 2 s may occur during eruptive or quiet phases at volcanoes of all types (shield and stratovolcanoes with calderas, as well as other stratovolcanoes) and are inherently connected to fluid movement within the plumbing system. This is supported by observations at several volcanoes that indicate a correlation between gas emissions and VLPs, as well as deformation episodes due to melt accumulation and migration that are followed by the occurrence of VLPs. Moment tensors of VLPs are usually characterized by large volumetric components of either positive or negative sign along with possibly the presence of single forces that may result from the exchange of linear momentum between the seismic source and the Earth. VLPs may occur during a variety of volcanological processes such as caldera collapse, phreatic eruptions, vulcanian eruptions, strombolian activity, and rockfalls at lava lakes. Physical mechanisms that generate VLPs include the inflation and deflation of magma chambers and cracks, the movement of gas slugs through conduits, and the restoration of gravitational equilibrium in the plumbing system after explosive degassing or rockfalls in lava lakes. Our understanding of VLPs is expected to greatly improve in the future by the use of new instrumentation, such as Distributed Acoustic Sensing, that will provide a much denser temporal and spatial sampling of the seismic wavefield. This vast quantity of data will then require time efficient and objective processing that can be achieved through the use of machine learning algorithms.

**Keywords** Very-long-period · Seismic signal · Active volcano · Moment tensor · Single force · Eruption

---

✉ K. I. Konstantinou  
kkonst@ncu.edu.tw

<sup>1</sup> Department of Earth Sciences, National Central University, Jhongli 320, Taiwan

## Article Highlights

- VLPs can be observed in a variety of volcanoes and their occurrence is inherently connected to the movement of hydrothermal or magmatic fluids through the plumbing system
- Moment tensor inversion of VLP waveforms has revealed large volumetric components and possibly significant single forces
- Physical mechanisms that have been employed to explain the generation of VLPs involve inflation and deflation of cracks and magma chambers, movement of gas slugs through conduits and restoration of gravitational equilibrium in lava lakes

## 1 Introduction

Seismic signals recorded at active volcanoes convey important information about the internal structure, state of stress as well as the nature and dynamics of the fluids within the volcanic system (Chouet 2003; Chouet and Matoza 2013). Volcano-tectonic earthquakes were the first to be studied due to the similarities they share with their tectonic counterparts, as both of them are generated by brittle failure of rock. Such events can be used in order to better understand the stresses that develop within volcanoes (Gerst and Savage 2002; Roman and Cashman 2006), as well as provide a warning of impending eruptions in the form of changes in seismicity rates (Kilburn and Voight 1998; Kilburn 2003; White and McCausland 2019; Duputel et al. 2019). On the other hand, Long-Period (LP) or hybrid earthquakes and volcanic tremor represent seismic signals that are generated through the complex interaction of fluids and gas with the solid rock and thus their source mechanism is much harder to decipher. Some source models for these events favor the mechanism of a crack that is driven to resonance due to fluid flow (Chouet 1996; Chouet and Dawson 2016 and references therein), while other models suggest that these signals can be also generated by the deformation of low-cohesion volcanic rock (Bean et al. 2014; Eyre et al. 2015; Rowley et al. 2021). Either way, all of these signals proved to be of great importance for elucidating the dynamics of fluid flow and the nature of the fluids involved (Chouet 1996; Kumagai and Chouet 2000; Kumagai et al. 2005). Beyond this, LP earthquakes and volcanic tremor are also valuable as monitoring tools since many eruptions are preceded by both types of signals (Konstantinou and Schlindwein 2003; Chouet and Matoza 2013).

Several decades ago the frequency range of volcano-seismic signals was thought to start at about 1 Hz extending to 20 or even 50 Hz and exhibiting considerable overlap between signals generated by brittle failure and those generated by fluid flow (Fig. 1). However, this view of volcanic seismicity was biased by the deployment in the field of short-period instruments that could reliably record frequencies of 1 Hz or higher. The advent of portable sensors with the ability to record frequencies as low as 0.00833–0.01 Hz and their installation at active volcanoes eliminated this observational bias and brought into sharp focus the fact that volcanoes are broadband sources of seismic energy. Since then Very Long Period (VLP) signals were detected at several volcanoes around the world, extending the frequency bandwidth of observed volcano-seismic signals down to at least 0.02 Hz and in some cases lower than 0.01 Hz (cf. Fig. 1). VLPs have been found to be associated with different volcanic processes that involve large-scale movement of fluids prior to or during eruptive activity, hence their study can potentially provide constraints on the fluid mass budget and dynamics inside active volcanoes.

This work presents an extensive review of the characteristics and source properties of VLPs placing emphasis on the observational aspects and physical mechanisms of their

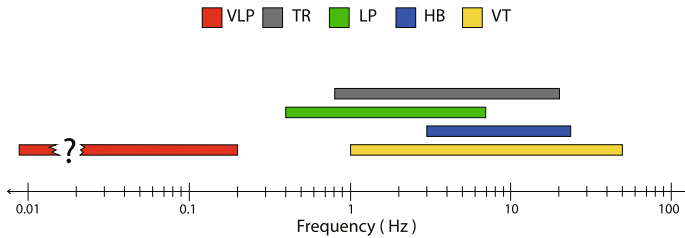


**Fig. 1** Diagram that depicts the frequency range of different classes of volcano-seismic signals based on the cited references. VT: volcano-tectonic earthquakes (White and McCausland 2019), HB: hybrid events (Harrington and Brodsky 2007), LP: long-period events (Chouet 1996), TR: volcanic tremor (Konstantinou and Schlindwein 2003), VLP: Very Long Period events (this study and references therein). The question mark in the VLP bar implies that detection of such signals with periods longer than 50 s is dependent on the instrument passband (see also Sect. 3.3.2)

occurrence. In the first part of this review, an account of the phenomenology of VLP occurrence is given in terms of their salient characteristics, their relationship with fluid movement, and whether their occurrence is affected by factors external to volcanic activity. Moment tensors are used in order to describe the source process of VLPs and this review examines the different methodologies utilized in moment tensor inversion, as well as the variability and properties of their moment tensors inferred from seismic data at several volcanoes worldwide. In the second part of the review the volcanological processes that are associated with VLPs are grouped into five categories and a description of the physical mechanisms in each category is given along with typical examples of active volcanoes where such mechanisms have been suggested to be at work. The last part presents a discussion that focuses on the potential use of machine learning techniques for detection and analysis of VLPs, as well as concluding remarks.

## 2 Phenomenology of VLPs

VLPs can be formally defined as seismic signals with period ranging from several to tens of seconds that occur at active volcanoes during eruptive or quiet periods, corresponding to a source that is non-destructive and is inherently connected to physical mechanisms of fluid movement within the plumbing system. The term Ultra Long Period (ULP) signal is sometimes used in the literature when the dominant period is in the order of hundreds rather than tens of seconds (e.g., Longo et al. 2012; Fontaine et al. 2019). Possibly the first observation of VLPs at an active volcano was provided by Kenzo Sassa in the early 1930s after the installation at Aso volcano, Japan, of long-period Wiechert seismographs that recorded such signals with a dominant period of 3.5–8 s (Kawakatsu et al. 2000). Observations of VLPs re-emerged many decades later, when Kawakatsu et al. (1994) recorded oscillations with a dominant period of 10 s at Aso initiating the search for VLPs at other volcanoes worldwide. Figure 2 shows a stacked waveform of hundreds of VLPs recorded at Erebus volcano, Antarctica, along with its corresponding amplitude spectrum where the separation of long-period peaks from the short-period band can be clearly seen. In this particular example the VLPs contain energy at 3 different periods (8, 11, 20 s), even though at other volcanoes they may exhibit only one dominant period.

VLPs have been recorded at different volcano types, namely shield volcanoes (SH/CA) and stratovolcanoes (SV/CA) hosting calderas as well as at other stratovolcanoes

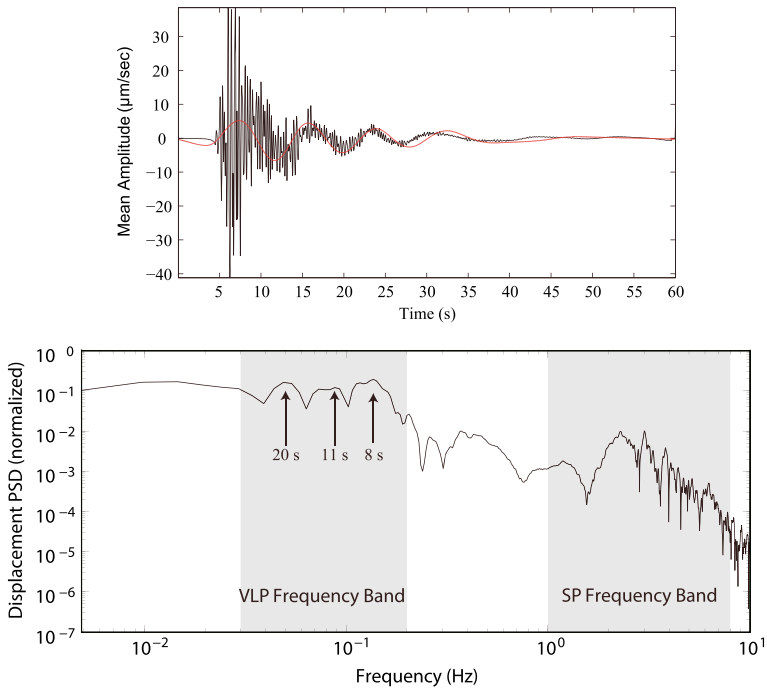


**Fig. 2** Top panel: velocity waveform produced by stacking of 1209 VLPs that occurred at Erebus volcano, Ross Island, Antarctica (after Knox et al. 2018). The red line is the trace of the stacked waveform after bandpass filtering between 0.03 and 0.2 Hz. Lower panel: power spectral density of the stacked waveform showing both the short-period and the VLP bands. The arrows highlight the three different periods of the VLP band (Knox et al. 2018)

(SV), all of which cover a wide range of tectonic and volcanological settings as can be seen in the world map of Fig. 3a. A look into the source depth and period of VLPs (this period refers to the period analyzed in each study) suggests a systematic pattern among the three volcano types (Fig. 3b). VLPs at stratovolcanoes with calderas appear to have the largest source depth at 1.5–3.5 km below sea level, while at shield and at other stratovolcanoes the VLPs source lies in most cases above sea level and within the volcano edifice. Stratovolcanoes and shield volcanoes with calderas seem to produce VLPs with periods up to 20 s in contrast to other stratovolcanoes where the reported period seems to be ranging from 3 s up to about 70 s. At this point it should be noted that VLPs at Kilauea exhibit a wide range of periods (2–40 s, hence the symbol in Fig. 3b is shown as a black inverted triangle not following the color scale) and while most occur at or above sea level depth (Dawson and Chouet 2014) some events have been observed down to depths of 8 km (Almendros et al. 2002). It is also important to stress that these inferences are subjected to three possible biases: first, most of the VLPs reported in the literature are recorded at stratovolcanoes (SV), while the other two volcano types (SH/CA and SV/CA) seem to be underrepresented; second, detailed analysis of VLPs is mostly limited to well-monitored volcanoes in developed countries (e.g., Kilauea in the United States), or at volcanoes associated with particularly high volcanic risk (e.g., Merapi in Indonesia). Third, even at volcanoes that are seismically monitored there may exist

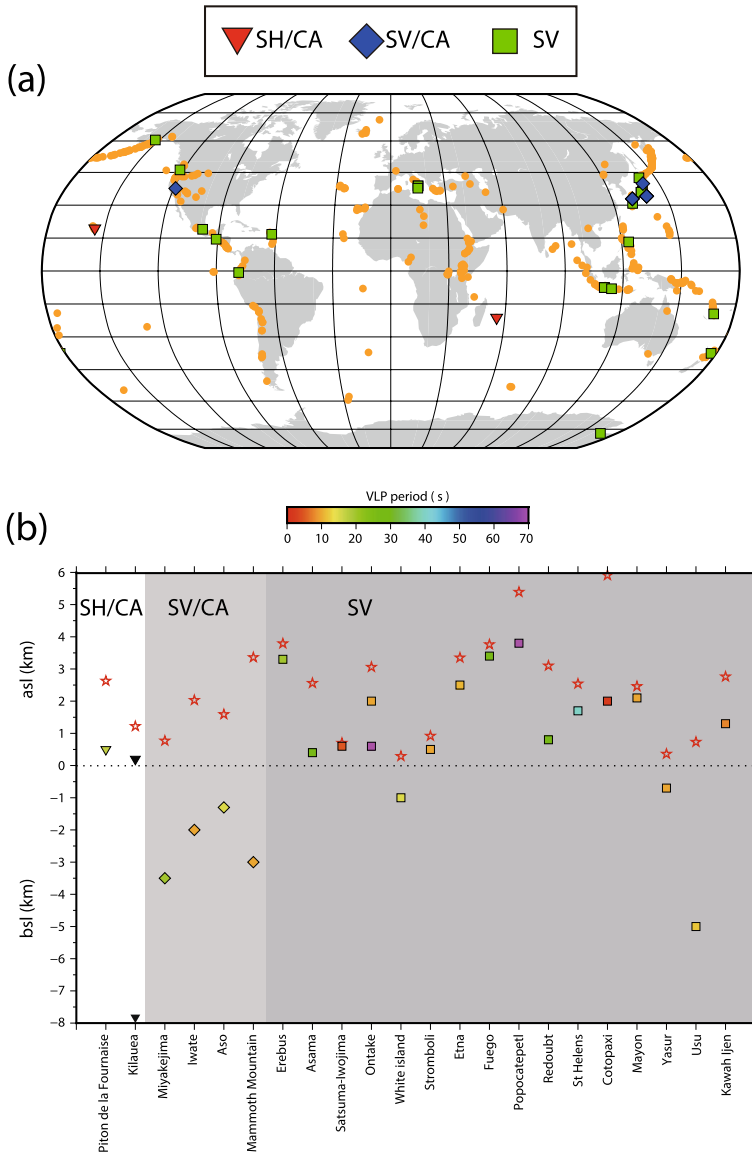


**Fig. 3** **a** Global distribution of volcanoes that exhibit VLP activity as found in the literature. Orange dots symbolize all active volcanoes worldwide according to the Smithsonian Institution database. Volcanoes that exhibit VLPs are shown as red triangles for shield volcanoes with calderas (SH/CA), blue diamonds for stratovolcanoes with calderas (SV/CA), and green squares for all other stratovolcanoes (the Smithsonian Institution typology is followed for each volcano); **b** Diagram that shows the relationship between the depth of VLPs extracted from the literature for different volcanoes (shown as squares) and the peak elevation of these volcanoes (shown as red stars). Each depth symbol is colored based on the period of VLPs according to the color scale shown on top (asl: above sea level, bsl: below sea level). Depth uncertainties are not plotted since in all cases they are smaller than 1 km and in most cases smaller than 500 m. For Kilauea the symbol is colored black for the reason that VLPs exhibit a range of dominant periods between 2 and 40 s and there are two VLP source depths, one near sea level (Dawson and Chouet 2014) as well as another near 8 km (Almendros et al. 2002). For Ontake there are also two different VLP sources, a deeper one located by Nakamichi et al. (2009), and a shallower one located by Maeda et al. (2015a) that occurred just prior to the 2014 phreatic eruption

VLPs with different properties that have not yet been properly studied. Table S1 in the supplementary information that accompanies this work contains the characteristics of VLPs shown in Fig. 3b.

Some observations relating VLPs and the movement of fluids within the plumbing system come from the comparison of seismic and gas monitoring data, even though to date such studies are available only at few volcanoes worldwide. At Asama volcano, Japan, VLPs recorded by broadband seismometers were usually followed by ash-free gas bursts near the active crater as monitored by a dedicated SO<sub>2</sub> imaging system (Kazahaya et al. 2011, 2015). The seismic moment calculated from VLP waveforms exhibited a positive linear correlation with SO<sub>2</sub> emissions, while the monthly emissions of SO<sub>2</sub> were also found to positively correlate with the monthly average product of the number of VLPs multiplied by their displacement amplitudes. In some cases such correlation was not as strong, for example (Zuccarello et al. 2013) reported that only a fraction (~5%) of VLPs correlated with the total SO<sub>2</sub> gas emissions recorded at Etna volcano in Italy. At other volcanoes the comparison between seismic and gas emission data was performed for smaller time periods, however, there was still a temporal correlation between an increased number of VLPs and vigorous degassing activity (Aster et al. 2003; Jousset et al. 2013; Waite et al. 2013; Ripepe et al. 2021). Observations relating VLPs with melt movement come from Aso volcano, Japan, where repetitive VLPs occur after deformation episodes (Niu and Song 2021a). These episodes were interpreted as the accumulation of melt near the roof of the Aso magma chamber, and the slow migration of this melt to a shallow conduit resulting in the generation of VLPs. Similar observations relating VLP signals with the flow of basaltic magma through a dike were also reported previously beneath Hachijo Island, Japan, by Kumagai et al. (2003). In conclusion, all of the aforementioned studies point to the suggestion that VLPs represent the seismic response of structural features (dikes, conduits) to fluid (melt, gas) movement within the plumbing system of each volcano. This suggestion can be further corroborated by the results of waveform inversion for the determination of VLP moment tensors that will be described in the next section.

Except from the internal dynamics of the volcanic system, other studies have investigated the possibility that the occurrence of VLPs may also be influenced by external factors. The first of these factors is large earthquakes that may occur near an active volcano, as was the case of the 2016 (Mw ~7) Kumamoto earthquake whose epicenter was located about 20 km from Aso volcano in Japan. Hendriyana and Tsuji (2019) reported that before the Kumamoto earthquake, VLPs at Aso occurred prior to phreatomagmatic activity and their locations formed a single tight cluster beneath the volcano. After the Kumamoto earthquake a migration of VLP activity was observed to another cluster to the west of the original one. The authors explained this migration as the result of enhanced permeability of the rocks beneath the volcano in the form of new cracks that were produced by static and dynamic stresses after the earthquake. Niu and Song (2021b) also observed increased VLP activity at Aso after the passage of surface waves generated by the 2011 (Mw ~9) Tohoku earthquake, where high dynamic stress is also thought to have enhanced rock permeability. The second of the external factors has to do with periodic loading caused by tides or meteorological phenomena such as rainfall and atmospheric pressure variations. A careful statistical comparison of the number of VLPs at Aso volcano with diurnal/semi-diurnal variation of tides, barometric pressure and rainfall showed that there was no significant correlation (Niu and Song 2021b).

### 3 The Seismic Source of VLPs

#### 3.1 Source Inversion Methodologies

As with other seismic signals such as earthquakes and man-made explosions, the recorded waveforms of VLPs can be utilized in order to determine the moment tensor that corresponds to the seismic source that generated them. The vast majority of the studies that perform moment tensor inversion of VLPs follow a point-source approximation and also consider that each moment tensor element may vary as a function of time. An additional factor that has to be considered in a volcanic environment is the presence of single forces that may result from the exchange of linear momentum between the seismic source and the Earth (Takei and Kumazawa 1994). In these cases momentum conservation dictates that the net exchange of linear momentum should cancel out, hence an upward acceleration or downward deceleration of the source volume will produce a downward reaction force on the Earth and the opposite will occur when there is a downward acceleration or upward deceleration (Chouet et al. 2003). Taking into account all these factors it is possible to express the recorded amplitude of VLPs as a function of time in the following way (e.g., Chouet and Matoza 2013 and references therein)

$$u_n(\mathbf{r}, t) = F_p(t) * G_{np}(\mathbf{r}, t) + M_{pq}(t) * G_{np,q}(\mathbf{r}, t) \quad (1)$$

where  $F$  represents the single force component,  $G$  is the Green's function describing the medium response at a receiver location  $\mathbf{r}$ ,  $M$  is the moment tensor,  $p, q$  are the directions of the Cartesian coordinate system ( $x, y, z$ ), and  $n$  is the component of displacement (Z, R, or T). In equation (1), the Einstein summation convention is used, where the summation is performed over the repeated indices. For a particular station component this expression can then be written in a compact form as

$$u_n(t) = \sum_{i=1}^k m_i(t) * G_{ni}(t) \quad (2)$$

where the index  $i=1, \dots, k=9$  refers to the number of six moment tensor elements and three force components. It is easy to transform the previous expression from the time to the frequency domain where convolution becomes multiplication and then obtain (e.g., Auger et al. 2006)

$$u_n(\omega) = \sum_{i=1}^k m_i(\omega) G_{ni}(\omega) \quad (3)$$

Using this equation it is then possible to obtain a matrix relationship  $\mathbf{d}(\omega) = \mathbf{G}(\omega)\mathbf{m}(\omega)$  where  $\mathbf{d}$  represents the vector of amplitudes for frequency  $\omega$ ,  $\mathbf{G}$  is the matrix containing the Green's functions for this frequency,  $\mathbf{m}$  is the vector containing the sought moment tensor elements and single force components. The solution of this linear problem can be obtained by minimizing the error between observed and synthetic amplitudes for each frequency. A large number of studies have performed such unconstrained source inversion (Ohminato et al. 1998; Hidayat et al. 2002; Chouet et al. 2003, 2005, 2010; Auger et al. 2006; Ohminato 2006; Waite et al. 2008; Aster et al. 2008; Lyons and Waite 2011; Chouet and Dawson 2011, 2013; Haney et al. 2013; Zuccarello et al. 2013; Waite and Lanza 2016; Jolly et al. 2017; Matoza et al. 2022).

Another inversion strategy that has been employed is constraining the VLP source to a specific geometry such as a rectangular crack or cylindrical pipe. In this case the inversion problem can be written as

$$\mathbf{d} = \mathbf{G}M_0\mathbf{f}(\lambda/\mu, \theta, \phi) \quad (4)$$

where  $M_0$  is the scalar moment,  $\lambda, \mu$  are the Lamé constants,  $\theta, \phi$  are angles defined by the Cartesian coordinate system and the assumed geometry of the source (Fig. 4). The reasoning behind the choice of such particular geometries is based on the fact that the VLP source is likely related to volcanological features such as a sill or dike and can be approximated by simple geometrical shapes. In this case each moment tensor element will be a function of the scalar moment, the Lamé constants and the angles  $\theta$  and  $\phi$  as depicted in the matrix of Fig. 4. The advantage of this approach is the reduction in the number of unknowns from 6 moment tensor elements to just three quantities ( $M_0, \theta, \phi$ ). This constrained source inversion has been performed in fewer studies (Molina et al. 2008; Nakamichi et al. 2009; Jousset et al. 2013; Maeda et al. 2015a, b), since a priori assumptions about the geometry of the VLP source are not always possible.

As stated earlier, the frequency content of VLPs is low enough so that propagation effects due to the small-scale heterogeneity have little influence on the recorded signal (at least for frequencies of 0.1 Hz and lower), therefore Green's functions can be calculated using simple half-space or layered velocity models that may also include the effects of volcano topography. Either inversion strategy requires one to know the source location of VLPs, that can be obtained independently by using waveform semblance (Kaneshima et al. 1996; Ohminato et al. 1998; Kawakatsu et al. 2000; Nishimura et al. 2000; Almendros et al. 2002; Yamamoto et al. 2002; Dawson et al. 2004; Cannata et al. 2009; Guidicepietro et al. 2009; Jolly et al. 2017), amplitude source location (Maeda et al. 2019), or by just incorporating the location into the source inversion problem and perform grid-search (Legrand et al. 2000; Chouet et al. 2003, 2005, 2010; Auger et al. 2006; Ohminato 2006; Waite et al. 2008; Aster et al. 2008; Nakamichi et al. 2009; Chouet and Dawson 2011, 2013; Lyons and Waite 2011; Maeda and Takeo 2011; Haney et al. 2013; Jousset et al. 2013; Maeda et al. 2015a, b; Šindijia et al. 2021). The latter approach can be realized by conducting a search over a dense grid of points beneath the

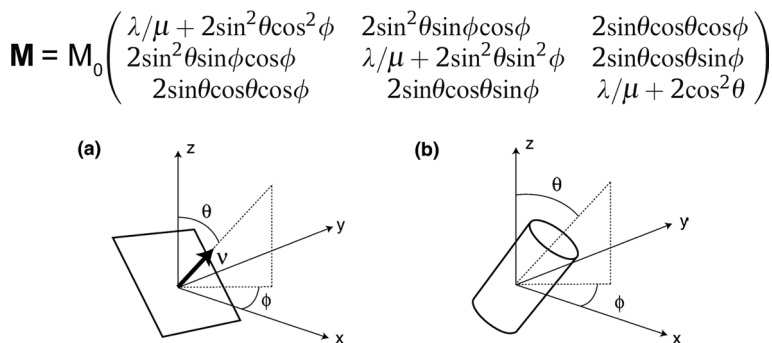


**Fig. 4** Potential geometry of VLP sources used in constrained inversions: **a** rectangular crack where the angles  $\theta$  and  $\phi$  are measured based on the orientation of vector  $\mathbf{v}$  which shows the direction of the crack opening or closing; **b** cylindrical pipe where the angles are measured using the vertical axis of the cylinder as reference. The general moment tensor that may correspond to either of these geometries is shown at the top of the Figure (see text for more details)



volcano with the aim of finding the source location that yields the vector **m** which best fits the observed waveforms.

### 3.2 Source Model Selection

In the case when the inversion determines moment tensor elements and single force components, it is customary to consider VLP sources that may correspond to only moment tensor elements, or a combination of moment tensor and single force components. Each of the two source representations entails a different number of parameters that need to be included in the inversion (3 moment tensor elements for a purely volumetric source, 6 elements for a full moment tensor and 9 elements if single forces are also considered). It is well known that increasing the number of parameters in an inversion problem will result in a better fit, however, it is not clear whether these extra parameters are really needed in order to explain the observed data. Most studies try to avoid this ambiguity by utilizing the Akaike Information Criterion (AIC), which can be defined as (Akaike 1974)

$$AIC = (N_t \times N_s) \log S + 2N_p \quad (5)$$

where  $N_t$  is the number of traces and  $N_s$  is the number of samples used in the inversion,  $S$  is the squared error between observed and synthetic data, and  $N_p$  is the number of free parameters determined by the inversion. AIC is usually calculated for each source representation and the solution that attains the smallest AIC value is considered as the more likely representation of the VLP source. A caveat related to the use of AIC has to do with the fact that its efficiency diminishes sharply once the squared error is not normally distributed (see van Driel et al. 2015). This may occur for a multitude of reasons such as the small number of available stations, poor azimuthal distribution, or a velocity model that deviates significantly from the actual velocity structure. The Bayesian Information Criterion (BIC) has been suggested as an alternative to AIC and its definition can be written as (e.g., O'Brien et al. 2010)

$$BIC = (N_t \times N_s) \log S + N_p \log (N_t \times N_s) \quad (6)$$

O'Brien et al. (2010) inverted synthetic seismograms generated by a variety of hypothetical sources in the LP frequency domain, under different station as well as velocity model conditions. The authors found that BIC performs better than AIC in selecting the correct source model, although BIC could still fail to select the correct solution if the number of stations is small ( $< 10$ ) or when single forces were included. Even though these synthetic tests were only applied to LP events, it is reasonable to assume that AIC may also fail to select the correct source model for VLPs and that BIC would perform better but it still would not be a foolproof solution. The next section describes some of the problems and limitations of source inversions in terms of the quality of data, instrument passband and the reliability of single forces in the derived source solutions of VLPs.

### 3.3 Problems and Limitations of Source Inversions

#### 3.3.1 Tilt Effects

Dynamic tilt is the rotational motion around the horizontal axis that changes the projection of local gravity onto the horizontal components of the seismometer sensor without

affecting the vertical component (Rodgers 1968; Wielandt and Forbriger 1999; Lyons et al. 2012). The resulting horizontal acceleration can then be expressed in differential form as (Aki and Richards 2002)

$$\ddot{u}(t) = -g\theta(t) \quad (7)$$

where  $\ddot{u}(t)$  is horizontal acceleration,  $g$  is acceleration of gravity, and  $\theta(t)$  is tilt-angle as a function of time. Integrating twice the above stated differential equation would yield the displacement of motion as the second integral of the tilt-angle time history. It can be shown that the effect of tilt is proportional to  $1/\omega^2$ , hence it is negligible for higher frequencies but quite significant for lower frequencies such as those observed in VLPs. Tilt effects influence the stations of a seismic network by a varying order of magnitude due to differences in the radiation pattern of the VLP source and the interaction of the seismic wavefield with the volcano topography.

The effect of tilt on the moment tensor inversion of VLPs was investigated by van Driel et al. (2015) using synthetic waveforms calculated for a homogeneous velocity model and utilizing the digital elevation model of Merapi volcano in order to include the effects of topography in a realistic way. Tilt was found to affect the source inversion of VLPs with dominant period longer than 10 s, even in the case when the tilt effect was apparent only in a small number of stations. One solution for minimizing the effect of tilt would be to calculate tilt Green's functions and then perform a joint inversion for both translation and rotation. The theoretical displacement for component  $n$  and receiver position  $\mathbf{r}$  in the frequency domain can be written as (Maeda and Takeo 2011; van Driel et al. 2015)

$$u_n(\mathbf{r}, \omega) = M_{pq}(\omega)[\tilde{I}_n(\omega)\tilde{G}_{np,q}(\mathbf{r}, \omega) + I_n(\omega)G_{np,q}(\mathbf{r}, \omega)] \quad (8)$$

where  $p, q$  are direction indices,  $M_{pq}$  is the  $pq$  component of the moment tensor,  $\tilde{I}, I$  are the tilt and translation instrument response (with  $\tilde{I} = gI(i\omega)^{-2}$ ), and  $\tilde{G}, G$  is the Green's functions for tilt and translation respectively. The inversion can be performed for each frequency separately by solving the linear problem  $\mathbf{u}(\omega) = \mathbf{G}(\omega)\mathbf{s}(\omega)$ , where  $\mathbf{s}(\omega)$  is the Fourier transformed moment tensor components that are sought. This approach can minimize significantly tilt effects and has been applied to the inversion of VLPs at a number of volcanoes such as Asama (Maeda and Takeo 2011), Stromboli (Chouet and Matoza 2013), Kilauea (Chouet and Dawson 2015), Fuego (Waite and Lanza 2016), and White Island (Jolly et al. 2017).

A potential drawback of this approach is that the Green's functions are not taking into account strain-rotation coupling that results from converting strain on the scale of the seismic wavelength to rotation on a local scale (Wielandt and Forbriger 1999; van Driel et al. 2012). Strain-rotation coupling is a local site effect, thus it will not be accounted for when the Green's functions are calculated for a homogeneous velocity model and smooth topography. A better solution for removing tilt, without the need for detailed knowledge of the velocity structure, would be the *in situ* correction of the affected seismograms with the recording of the 3 components of rotation. This would require the installation in the field of 6 degrees of freedom sensors (3 components for translation motion and 3 components for rotation) which are still not widely available. However, prototypes of such sensors have already been tested in volcanic environments (e.g., Wassermann et al. 2022) hence this kind of corrections will be possible in the near future.

### 3.3.2 Artifacts Due to the Instrument Passband

VLPs characterized by periods tens of seconds long are to be expected during a process such as caldera collapse, where large scale subsidence and magma chamber expansion or contraction are involved (cf. Sect. 4.1). The 2018 caldera collapse at Kilauea was probably the best documented so far and its accompanying phenomena were recorded by near-field seismic sensors (Streckeisen STS2, Trillium 120 s, Güralp CMG-40T) as well as co-located GPS receivers and tiltmeters. The displacement signal of each incremental collapse was recorded as a ramp function by GPS receivers and their similarity made possible the stacking of these signals producing a master ramp function with duration of  $26 \pm 5$  s (Flinders et al. 2020). When this ramp function is convolved with the instrument response of a broadband seismometer the result is a pulse-like seismogram depicting a VLP event with a period  $T_0$  that is proportional to the duration of the ramp function (Fig. 5). Prior to moment tensor inversion it is common practice to use a zero-phase bandpass filter in order to restrict the useful signal around the passband of the instrument and then deconvolve the instrument response. Unfortunately this leads to a distorted displacement seismogram, whose period  $T$  is now longer than the original period  $T_0$ .

The reason behind this artifact is that the ramp function corresponds to a sinc-function in the frequency domain, which cannot be fully recovered after deconvolution since part of it falls below the low-frequency corner of the instrument ( $\sim 50$  s). Flinders et al. (2020) suggest that in such cases it is critical to have co-located GPS and seismic stations in order to be able to compare synthetic seismograms derived from the GPS displacement and observed VLP seismograms after deconvolution. So far this issue has not received much attention in the literature, even though Flinders et al. (2020) speculate that similar artifacts may be present in VLP waveforms recorded during previous caldera collapses (Miyakejima, Piton de la Fournaise, see Sect. 4.1). Future studies should explore the influence of such artifacts on the results of moment tensor inversion, in terms of inferred volume change and the amplitude of single forces.

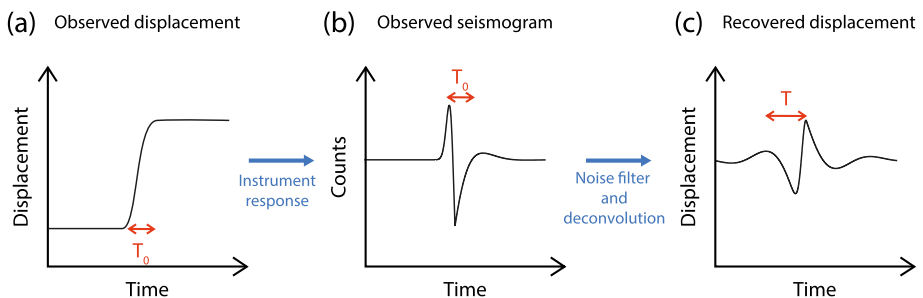


**Fig. 5** Diagram that illustrates the distortion caused to displacement waveform due to limited instrument bandpass (after Flinders et al. 2020): **a** ramp function displacement of caldera collapse with duration  $T_0$  as it would be recorded by a near-field GPS receiver, **b** observed velocity seismogram of the same process, and **c** distorted displacement waveform of caldera collapse after noise filtering and deconvolution, exhibiting period  $T > T_0$

### 3.3.3 Spurious Single Forces

Several studies have included in their inversion formulation the existence of single forces and have utilized AIC in order to determine whether the increase in free parameters leads to a significantly better data fit. Besides the problems related to the use of AIC (cf. Sect. 3.2), this procedure cannot answer the question of whether single forces are real or an artifact of the inversion, and under which conditions can such an artifact occur. A number of studies tried to tackle this issue by performing synthetic tests not only for the case of VLPs, but also for higher frequency ranges ( $> 0.2$  Hz) that correspond to LP events (Ohminato et al. 1998; Bean et al. 2008; Davi et al. 2010; De Barros et al. 2013; Trovato et al. 2016). These tests calculated synthetic waveforms assuming both shallow and deep sources, with and without the presence of single forces, and with variable noise level. The synthetic waveforms were then inverted using different scenarios of inaccurate velocity models and mislocated sources. The results of these tests have shown that spurious single forces may appear due to three factors: (1) signal-to-noise ratio  $\leq 2$ , (2) vertical mislocation of the source by hundreds of meters, and (3) the presence of shallow low-velocity layers often found at volcanoes, that are usually not accounted for in velocity models used to calculate Green's functions.

While the effect of an inaccurate velocity model on the source inversion results is expected to be small in the case of VLPs, vertical mislocation may still produce spurious single forces. VLPs are particularly prone to such mislocation for two reasons: first, as shown in Fig. 3b most of the VLP sources are quite shallow, hence lack of knowledge of the shallow structure (which is the case in most volcanoes worldwide) is likely to lead to such mislocation. Second, VLP wavelengths are usually much longer than the source-receiver distance, hence the accuracy of the obtained location depends critically on near-field effects (Lokmer and Bean 2010). Two practical recommendations were put forward by the aforementioned studies in order to avoid spurious single forces: (1) prior to the inversion of the real data, synthetic tests should be performed in order to infer whether single forces can be recovered with the given station distribution, noise level and velocity model; and, (2) that the VLP source location has to be performed using a technique that is less sensitive to the choice of the velocity model (e.g., waveform semblance).

### 3.4 Moment Tensors of VLPs: An Overview

At this point it would be useful to obtain an overview of VLP moment tensors before discussing any particular physical mechanism for their generation. A graphical depiction of a set of moment tensors can be realized by using the fundamental lune representation suggested by Tape and Tape (2013). In this representation the three eigenvalues of each moment tensor are utilized for the purpose of calculating the following quantities

$$\beta = \cos^{-1} \left( \frac{\Lambda_1 + \Lambda_2 + \Lambda_3}{\sqrt{3} \|\Lambda\|} \right) \quad (9)$$

$$\gamma = \tan^{-1} \left( \frac{-\Lambda_1 + 2\Lambda_2 - \Lambda_3}{\sqrt{3}(\Lambda_1 - \Lambda_3)} \right) \quad (10)$$

where  $\Lambda_1 > \Lambda_2 > \Lambda_3$  are the three eigenvalues and  $\|\mathbf{\Lambda}\| (= \sqrt{\Lambda_1^2 + \Lambda_2^2 + \Lambda_3^2})$  is the Euclidean norm of the moment tensor. Hence a moment tensor can be plotted in the fundamental lune by calculating  $\gamma$ , which is equivalent to longitude, and  $90^\circ - \beta$ , which corresponds to co-latitude. Using the eigenvalue information it is also possible to calculate the Poisson ratio  $\nu$  at the source as given for the classic model of a moment tensor (Tape and Tape 2013)

$$\nu = \frac{\Lambda_2}{\Lambda_1 + \Lambda_3} \quad (11)$$

Unfortunately not all published studies provide the triplet of eigenvalues or adequate information in order to calculate the eigenvalues from the moment tensor, therefore only 21 VLPs that occurred at 13 volcanoes were utilized (see Table S2 in the supplementary information). Despite this problem the graphical representation of the moment tensors, their seismic moment, as well as the Poisson ratio can provide insights prior to discussing suggested physical mechanisms.

The fundamental lune includes source representations that range from purely volumetric such as explosion (+ISO) and implosion (−ISO), to purely deviatoric such as Compensated Linear Vector Dipole (CLVD) and Double Couple (DC), while opening or closing tensile cracks (+C or −C) correspond to combinations of explosion or implosion with Linear Vector Dipoles (LVD). Figure 6 shows two versions of the fundamental lune where in the one of them VLPs are plotted as a function of the logarithm of seismic moment ( $\log M_0$ ), and in the other as a function of the corresponding Poisson ratio ( $\nu$ ). The majority of VLPs are plotted in the upper half of the fundamental lune indicating sources that represent an opening tensile crack and progressively shift to pure volume increase independently of the volcano type. Four VLPs that occurred at Piton de la Fournaise and Aso represent sources where a closing tensile crack or volume decrease is the dominant source process. Only one VLP event that occurred at Soufrière Hills volcano (Montserrat Island) seems to exhibit other significant components (DC, LVD) except from the volumetric one. From the diagram in Fig. 6a it can also be seen that the seismic moment of these VLPs ranges from  $10^{10}$  N m for a VLP event at Satsuma-Iwojima volcano related to passive degassing activity, to about  $10^{17}$  N m for an event related to caldera collapse at Piton de la Fournaise volcano. However, the range of seismic moment for the majority of VLPs is narrower and lies between  $10^{11}$ – $10^{14}$  N m (see Table S2).

In the fundamental lune the line that connects the opening and closing tensile cracks corresponds to  $\nu = 0.25$ , therefore it would be expected that the moment tensors of VLPs should be scattered around this line. This expectation reflects the fact that most crustal rock types exhibit Poisson ratios in the range between 0.1 and 0.4 and  $\nu = 0.25$  represents an average value for a Poisson solid (Gerçek 2007). Even though a small number of VLPs are indeed located near this line (Fig. 6b), the majority displays  $\nu$  above 0.35 and a few of them even above 0.5 (VLPs at volcanoes Miyakejima, Soufrière Hills, White Island, Aso), which is the maximum value that is plausible for crustal rocks. Most of these anomalous Poisson ratios correspond to VLPs that have occurred at stratovolcanoes, however, the sample is small enough to preclude drawing firm conclusions about such dependencies. The Poisson ratios shown here for VLP sources are in agreement with those presented by Tape and Tape (2013) for moment tensors corresponding to various seismic sources (natural earthquakes, man-made explosions, cavity or mine collapses) that also deviate significantly from a Poisson solid.

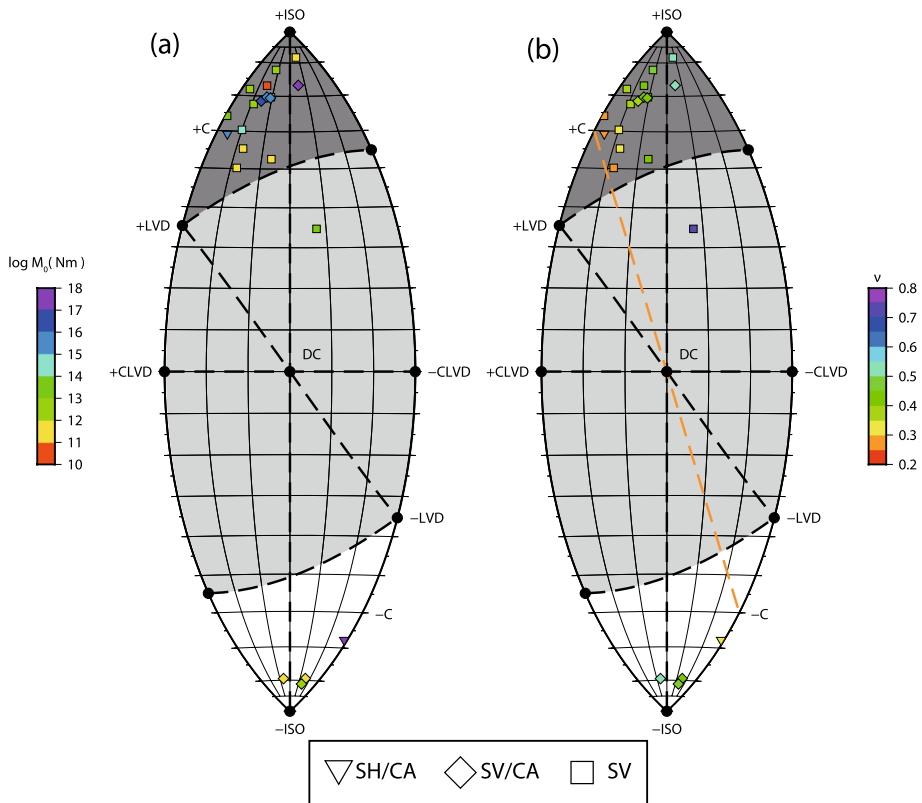


**Fig. 6** Fundamental lunes that depict the variation of the VLP source as a function of: **a** seismic moment, where the color of each symbol corresponds to the scale shown at the left part of the graph, and **b** Poisson ratio, where the color of each symbol corresponds to the scale shown at the right part of the graph. The dashed orange line represents the loci of sources with Poisson ratio equal to 0.25 (see text for more details). All other symbols are the same as in Figure 3

Even if Poisson ratios above 0.5 are discarded, there are still many VLPs whose  $\nu$  appears to be significantly different from the average value for crustal rocks. In the sample presented here (see Table S2 in the supplementary information), the two shield volcanoes with calderas (Kilauea, Piton de la Fournaise) seem to have Poisson ratios closer to the average (0.27–0.31), while the majority of VLPs at stratovolcanoes with calderas and other stratovolcanoes exhibit Poisson ratios above 0.4 (~64% different from a Poisson solid). The Poisson ratio is an important parameter for the reason that it can be used to express the relationship between the Lamé constants as (Mavko et al. 2009)

$$\frac{\lambda}{\mu} = \frac{2\nu}{1-2\nu} \quad (12)$$

which is essential when one needs to estimate the volume change  $\Delta V$  of an isotropic seismic source, since the equation commonly used for this estimation contains both constants (Müller 2001)

$$\Delta V = \frac{M_0}{\lambda + 2\mu} \quad (13)$$

In volcanological studies it is usually assumed that the Poisson ratio is equal to 0.33, a value that is considered appropriate for volcanic rocks at or near liquidus temperatures (Murase and McBirney 1973), thus  $\lambda \approx 2\mu$ . This means that for a VLP event with seismic moment  $10^{14}$  N m, taking the rigidity modulus as 10 GPa, and  $\nu = 0.33$ , the volume change will be equal to  $2500 \text{ m}^3$ . On the other hand, if  $\nu = 0.41$  (the median value of all Poisson ratios in Table S2) then  $\lambda \approx 4.6\mu$  and the volume change will be  $1515 \text{ m}^3$  (a difference of  $-40\%$  compared to the previous estimate). From a practical point of view, it is fair to say that such an estimation of volume change suffers not only from the uncertainties in the calculation of seismic moment, but also from the uncertainty in finding a plausible value for the Poisson ratio. Volume changes estimated in this way should be viewed with caution, and their interpretation in terms of the volcano's fluid mass budget should be cross-checked using available geodetic or gas emission data. The discrepancy between the commonly assumed Poisson ratio and the one implied by the moment tensors of VLPs is a point that has so far received very little attention in the literature. One explanation for this discrepancy is that it is an artifact stemming from a combination of factors such as poor station coverage, propagation effects not properly accounted for, and the inversion method utilized. While in some cases these factors may have played a significant role in producing anomalous Poisson ratios, it is doubtful that they represent the sole cause for all of them. Future studies should therefore try to investigate to what extent these factors are responsible for Poisson ratios much larger than 0.25 and also look for other potential causes.

## 4 Volcanological Setting and Physical Mechanisms

### 4.1 Caldera Collapse

The largest calderas on Earth were formed when massive magma chambers were evacuated after erupting most of their melt, which in turn resulted in the catastrophic collapse of the overlying rock column (Gudmundsson 2015 and references therein). During the last two decades four caldera collapses have been observed by modern instrumentation namely the 2000 Miyakejima, Japan (Kumagai et al. 2001), 2007 Piton de la Fournaise, Reunion Island (Fontaine et al. 2019; Duputel and Rivera 2019), 2014–2015 Bárðarbunga, Iceland (Gudmundsson et al. 2016) and 2018 Kilauea, Hawaii (Neal 2019; Anderson et al. 2019). A conceptual model that has been utilized in order to describe all four of the aforementioned caldera collapses is shown in Fig. 7a. In this model a system of steeply dipping ring faults controls through friction the movement of a rock column (hereafter called ‘piston’) that overlies an elliptically shaped magma chamber filled with melt. If the overpressure inside the magma chamber exceeds the tensile strength of the surrounding rock, a lateral magma intrusion may lead to a small eruption that will remove a fraction of melt from the magma chamber. Alternatively, the small eruption may occur if the frictional resistance along the ring faults is lowered (for example through percolation of hydrothermal fluids), allowing the piston to move downwards and thus increase the pressure inside the magma chamber. The result of either of these scenarios is the initiation of a feedback process where the chamber deflates due to magma outflow favoring further downward movement of the piston that will squeeze more magma out of the chamber deflating it even more. An important

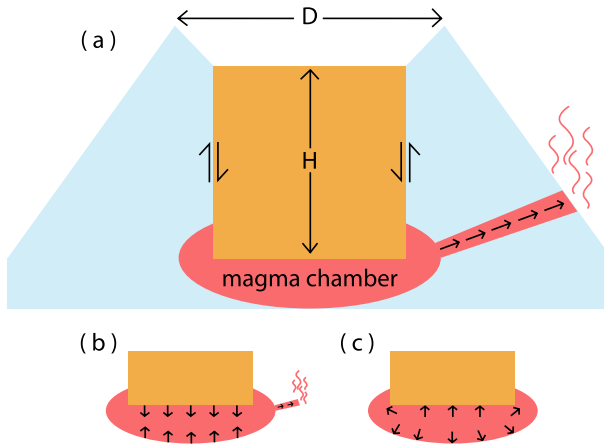


**Fig. 7** Diagram that describes the basic parts of the piston model for caldera collapse: **a** the movement of the piston is controlled by the frictional properties of the bounding faults. The pressure imposed by the downward moving piston will induce an increase in the overpressure of the magma chamber leading to an eruption. The horizontal extent of the caldera is equal to  $D$  and the vertical extent of the piston is  $H$ , where both quantities define the roof aspect ratio  $R$  (see text for more details), **b** the chamber may deflate if there is first an eruption which will then induce a downward piston movement, and **c** the chamber may inflate if the piston first moves downwards while there is no eruption prior to that

parameter of the piston collapsing model is the roof aspect ratio  $R$  defined as the fraction of roof depth to the piston diameter (cf. Fig. 7a). For  $R < 1.0$  the piston is expected to collapse as a coherent block whereas for larger values of  $R$  there is surface subsidence concurrently with collapse at depth (Fontaine et al. 2019; Anderson et al. 2019).

VLPs associated with caldera collapse have been recorded during the Miyakejima as well as during the Piton de la Fournaise collapses and their source process have been studied using moment tensor inversion. The Piton de la Fournaise caldera collapse took place incrementally producing 48 individual events that were accompanied by VLPs whose waveforms exhibited a high degree of similarity indicating that the same physical process generated these signals (Fontaine et al. 2019). The moment tensor of the largest of these VLPs, assuming a point-source approximation, showed a dominant volumetric decrease and a significant single force pointing upwards (Fontaine et al. 2019; Duputel and Rivera 2019). These results are consistent with the collapsing piston model, in the sense that the downward movement of the piston squeezed the magma chamber decreasing its volume (see also Fig. 6), while the downward acceleration of the piston block produced an upward vertical force. The Miyakejima caldera collapse was also accompanied by VLPs with dominant periods of 20 s and 50 s, however, the moment tensor displayed a dominant volumetric increase unlike the VLPs at Piton de la Fournaise (Kumagai et al. 2001; Kobayashi et al. 2012; Munekane et al. 2016). This difference can be explained based on the fact that in Piton de la Fournaise the piston movement was triggered after some melt had already been erupted, while in Miyakejima it was the piston movement that pressurized the chamber triggering subsequently an eruption (cf. Fig. 7b, c).

Fontaine et al. (2019) suggested that whether or not VLPs will occur during caldera collapse may depend primarily on the roof aspect ratio, since both Miyakejima and Piton de la Fournaise had an estimated  $R$  between 1.9 and 4.25, while for Bárðarbunga and Kilauea the estimated values of  $R$  were in the range of 0.3–1.6. This suggestion seems to agree well



with the fact that thus far there is no evidence that the Bárdarbunga collapse produced any VLPs. However, it is still not clear whether this is the result of the limited station coverage at the time, or the overlap of VLP frequency band with that of ambient noise which is abundant in Iceland and could have hindered the detection of VLPs. On the other hand, at Kilauea the first 12 detected VLPs were related to shallow draining of the lava lake and rockfalls (Anderson et al. 2019), whereas the remaining 50 events were directly related to the caldera collapse (Segall et al. 2019). Therefore more case studies are needed in order to understand the exact relationship between VLPs generation during caldera collapse and the roof aspect ratio.

Finally, VLPs generated by a variation of the caldera collapse mechanism have been reported by Cesca et al. (2020) offshore Mayotte Island in the western Indian Ocean. Similarly to the previous cases about  $1.3 \text{ km}^3$  of melt vacated a deep ( $\sim 25 \text{ km}$ ) magma chamber causing the progressive failure of the chamber roof. This produced a pressure pulse that triggered waves along the fluid-solid interface of the chamber's roof, resulting in the generation of 407 VLP signals with dominant periods 15.2–15.6 s and duration of several hundred seconds. The main difference of such VLPs with signals generated during other caldera collapses lies in the much greater depth of the VLP source, the extraordinarily long duration of the signal, and the fact that the roof collapse was facilitated by newly formed, distributed faults, rather than a pre-existing system of ring faults.

## 4.2 Phreatic Eruptions

The interaction of magma with water residing in the shallow aquifer beneath the volcano or in the hydrothermal system often leads to the sudden vaporization of water and its explosive discharge on the surface, producing in this way a phreatic eruption (Stix and Maarten de Moor 2018 and references therein). The products of such an eruption usually do not contain any juvenile material and the eruption intensity depends on many factors including the size of the hydrothermal system, its depth, and the size and dynamic state of the magma body (if it is ascending or it is static). VLPs have been observed prior to phreatic eruptions at a number of volcanoes in Japan such as Aso (Kaneshima et al. 1996; Kawakatsu et al. 2000; Legrand et al. 2000), Asama (Maeda and Takeo 2011; Maeda et al. 2019), Ontake (Nakamichi et al. 2009; Maeda et al. 2015a), as well as Kawah Ijen in Indonesia and White Island in New Zealand (Caudron et al. 2018), while at Mayon volcano in the Philippines one VLP event was observed concurrently with a phreatic eruption (Maeda et al. 2015b). In all of these cases the location of the VLP source was found to lie beneath the active crater at a depth that ranges from 100 m down to 1.3 km below the surface (cf. Fig. 3b). Moment tensor solutions of these VLPs have revealed large volumetric components and in most cases the data could be explained without the presence of a single force (see Table S2 and Fig. 6). An exception to this pattern was the VLP event at Mayon where a downward single force was required by the data and was interpreted as a force opposite to that of the explosion, since it occurred during the phreatic eruption (see Maeda et al. 2015b).

Many of the volcanoes where VLPs have been observed prior to or during phreatic activity exhibit a shallow plumbing system as the one shown in Fig. 8. In such a configuration the magma chamber provides heat and fluids (in the form of exsolved gases) to the shallow hydrothermal system that is represented as a reservoir consisting of permeable rock. Through fluid circulation the rock becomes chemically altered and the top of the reservoir is progressively sealed with the deposition of silica, clay, and zeolite minerals, ultimately resulting in the buildup of overpressure. Once the overpressure exceeds the tensile strength

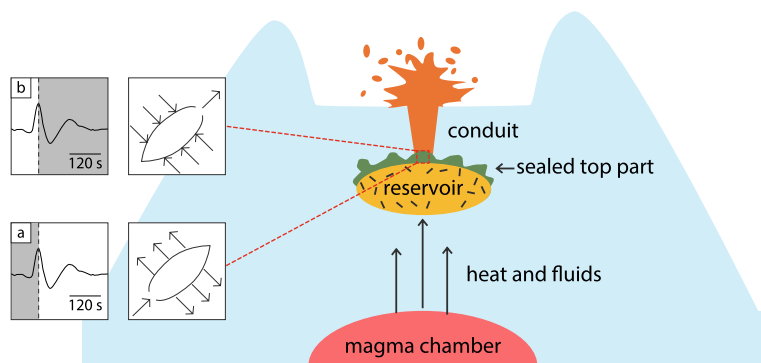


**Fig. 8** Configuration of the plumbing system of a volcano that is capable of producing phreatic eruptions. Heat and fluids from the magma chamber feed the shallow hydrothermal reservoir, while its top part is progressively sealed by the deposition of minerals. VLPs may occur once a crack develops at the top of the reservoir and fluid first causes the crack to inflate producing the compressional phase of the VLP waveform (a), and then the fluid leaves the crack, which subsequently deflates producing the dilational phase of the VLP waveform (b). The VLP waveform shown in this Figure was recorded at Ontake volcano prior to a small phreatic eruption (after Nakamichi et al. 2009)

of the rock, cracks may develop that transfer fluids to the conduit in order to be mixed with rock fragments and get erupted in the surface. Water is the dominant component of the fluids inside the crack with some fraction being of magmatic origin, while another fraction may be meteoric, since some volcanoes have a well-developed aquifer, or they host a crater lake as, for example, Aso volcano (Kaneshima et al. 1996; Niu and Song 2021a, b). Source characteristics of VLPs in the aforementioned volcanoes indicate that their generation consists of two phases: the phase of crack inflation when superheated water suddenly vaporizes and increases the crack volume, followed by the phase of crack deflation when the water vapor is discharged from the other side of the crack into the conduit. Figure 8a, b shows a comparison of these two phases with the waveform of a VLP event that occurred prior to a phreatic eruption at Ontake volcano (after Nakamichi et al. 2009), where compression corresponds to inflation and dilatation coincides with deflation of the crack. In some instances, VLPs have preceded phreatic eruptions for example at Asama (Maeda et al. 2019) and Ontake volcano (Nakamichi et al. 2009; Maeda et al. 2015a), therefore early detection of such signals could help efforts to provide warning ahead of the eruption.

### 4.3 Strombolian Eruptions at Stratovolcanoes

Strombolian activity is the most common type of explosive eruption that involves gas-rich, low-viscosity magma and it is frequently accompanied by the occurrence of VLPs. Stromboli volcano in Italy is the primary volcanic center where such eruptive activity has been recorded using different monitoring techniques such as seismic, infrasound, geodetic, thermal imagery, and time-lapse cameras. This has allowed the cross-examination of a variety of datasets in order to pinpoint the physical processes that are responsible for the generation of VLPs (Chouet et al. 2003; Auger et al. 2006; Guidicepietro et al. 2009; Ripepe et al. 2021; McKee et al. 2022; Legrand and Perton 2022). A widely utilized mechanism that is employed in order to explain strombolian activity has to do with the coalescence of gas bubbles into a large slug and its ascent through a conduit prior to bursting at the surface. This mechanism has been shown to occur in laboratory experiments (James et al. 2004,

2006) and it has also been associated with the generation of seismic signals of a wide frequency range in numerical simulations (O'Brien and Bean 2008).

The aforementioned studies highlighted the influence that the formation and ascent of large gas slugs have on strombolian activity and also contributed towards formulating specific physical models for VLP event generation. In the first of these models, a large gas slug transits through the base of the shallow volcanic conduit causing pressure to increase at its front and decrease at its rear (Fig. 9a). This will generate a seismic response in the form of a VLP event, but it will not produce any synchronous infrasound signal (such a signal may be produced later when the slug ascends to the surface and bursts). A mechanism of this kind has been invoked by Chouet et al. (2003) as a means of explaining VLPs occurring at Stromboli, in conjunction with a specific crack geometry at the base of the conduit derived from moment tensor inversion. A similar mechanism can also produce VLPs when the crack connects two magma reservoirs, rather than a magma reservoir and the surface. As the slug transits from the deeper to the shallower reservoir, it passes through the crack and may generate VLPs by slowly inflating and deflating the crack. These VLPs are usually accompanied by cyclic tilt changes and they have been observed at Kilauea (Ohminato et al. 1998), Iwate (Nishimura et al. 2000), Usu (Yamamoto et al. 2002), and Mammoth Mountain (Hill et al. 2002).

The second model has to do with the formation of a separate layer at the top of the conduit that may represent a crystal-rich or foam-rich melt zone that acts as a semi-solid plug. In this model the slug ascends aseismically until it reaches the base of the semi-solid plug where it fragments (Fig. 9b) and the pressure disturbance that is generated will propagate downwards toward the base of the conduit as a crack wave (Ferrazzini and Aki 1987). A crack wave may develop in the solid–fluid interface due to elastic coupling, when the solid behaves out-of-phase with the liquid (when the liquid expands, the solid contracts and vice versa). The effect of this is that the effective bulk modulus of the fluid is reduced, thus the speed of the crack wave becomes smaller than the sound speed of either the fluid or the solid. The VLP source lies at the bottom of the conduit and corresponds to the seismic response to this disturbance, again without producing any synchronous infrasound signals.

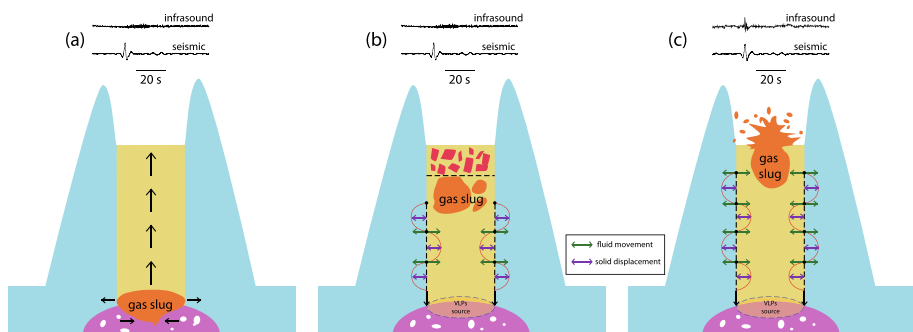


**Fig. 9** Three different models that are used in the literature in order to explain the generation of VLPs during strombolian eruptions: **a** a large gas slug transits through the base of a volcanic conduit up to the surface where it bursts, **b** the gas slug fragments after interacting with a semi-solid plug at the top of the conduit producing a downward propagating crack wave that excites the VLP source at the base of the conduit, and **c** the gas slug rises to the top, bursts and initiates a crack wave that excites the VLP source at the base of the conduit. Only in the last model there is an infrasound signal produced by the slug burst that is synchronous with the VLPs. Seismic and infrasound waveforms shown in this Figure have been adopted from Matoza et al. (2022)

Finally, in the third model the slug also ascends aiseismically to the surface where it bursts, creating a pressure disturbance that propagates downwards as a crack wave, triggering the VLP source at the bottom (Fig. 9c). This mechanism will generate VLPs as a seismic response to the pressure disturbance and the slug burst will also generate a synchronous infrasound signal.

A mechanism that combines elements of the second and third model has been proposed by Ripepe et al. (2021) after jointly examining seismic, infrasound, geodetic and thermal imagery data recorded during eruptions at Stromboli. For VLPs that occur after the slug burst, it was observed that their timing correlates well with high radiance during the explosions as well as with the high volumetric flux of gas. These observations imply that the VLP source may be located within the top 250 m of the magma column, hence the occurrence of these VLPs corresponds only to the final stage of slug ascent through the conduit. Based on these observations, Ripepe et al. (2021) suggested a model where the gas slug is formed above the column of crystal-rich melt, rising aiseismically until it reaches the top 250 m of the conduit. At that point the slug exerts pressure on the conduit walls which is transmitted in the solid medium and corresponds to the initial compression seen in the VLP waveform (phase A1 in Fig. 10). The slug then bursts resulting in pressure reduction and a sharp dilatation, followed by an oscillating coda that signifies the evolving equilibrium between the melt and the crystal-rich mush below (phases A2 and A3 in Fig. 10).

Recently two field experiments at Stromboli and Yasur volcano in Vanuatu have shed more light on the frequency of occurrence of VLPs related to the second and third models.

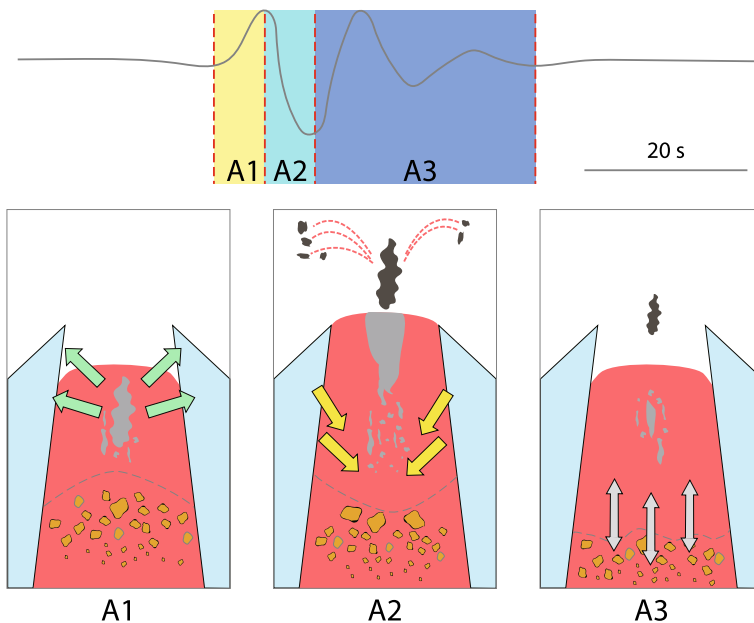


**Fig. 10** Model that was utilized in order to explain the generation of VLPs at Stromboli volcano (after Ripepe et al. 2021). Gas rises from the crystal-rich melt column and pressurizes the conduit generating the compression phase of the VLPs (A1). The gas is released in the atmosphere hence pressure in the conduit decreases and this generates the dilatational phase of the VLPs (A2). Oscillatory movement of the crystal-rich melt inside the conduit is responsible for the VLPs later coda (A3)

McKee et al. (2022) reported observations from a one-week field experiment at Stromboli, where the majority (~92%) of recorded VLPs did not coincide with infrasonic signals produced by slug bursts (hence the term ‘silent VLPs’). The authors proposed a mechanism where silent VLPs can be generated not by the breakup of a large gas slug, but due to the slow passage of gas through the semi-solid plug at the top of the conduit. They also suggested that the VLPs that are accompanied by infrasound signals can be explained by the same mechanism with the difference that gas bubbles this time have larger overpressure, thus they can ascend through the semi-solid plug and burst. Matoza et al. (2022) conducted a field experiment at Yasur of about the same duration and also reported that many VLPs lacked any accompanying infrasound signals. Their interpretation of this observation is generally based on the models described in Fig. 9b, c along with a particular dual crack or dual pipe geometry derived from moment tensor inversion. Undoubtedly, the most interesting observation from both studies is the apparent dominance of VLPs without synchronous infrasound signals which points to the existence of a crystal-rich, semi-solid zone at the top of the conduit. Longer deployments of such field experiments would help determine with greater certainty the percentage of ‘silent VLPs’ and allow to put more constraints on the interaction mechanism of ascending gas and the semi-solid plug at the top of the conduit.

#### 4.4 Vulcanian Eruptions

Vulcanian eruptions involve magma with higher viscosity that may form solidified plugs on top of the conduit or may extrude as a lava dome resulting in more explosive behavior. VLPs have been found to accompany vulcanian or dome building activity at several volcanoes, namely Fuego in Guatemala (Lyons and Waite 2011), Merapi in Indonesia (Hidayat et al. 2000, 2002; Jousset et al. 2013), Mt St Helens in NW United States (Waite et al. 2008), Popocatepetl in Mexico (Chouet et al. 2005) and Redoubt in Alaska (Haney et al. 2013). While in all of these volcanoes the source properties of VLPs appear similar, with large volumetric components and occasionally single forces, there is an important difference regarding their location and waveform similarity. At Merapi the VLPs were located inside the extruding lava dome and their waveform similarity degraded over time, signifying that the cracks inside the dome progressively opened or closed due to sealing. On the contrary, at the other volcanoes the VLPs exhibited a high degree of similarity throughout the study period that indicates a repeating and stable generation mechanism. In these cases the geometrical interpretation of the VLP source has to do with one vertical crack connected to a subhorizontal one, that may represent a dike-sill system. These observations highlight that the VLP source in these volcanoes corresponds to a stable geometrical configuration deep within the volcano edifice.

#### 4.5 Strombolian Eruptions and Rockfalls at Lava Lakes

Lava lakes represent vents within large volcanic systems where lava accumulates and remains in a mobile state for extended periods of time due to fluid and heat convection between the lake and a deeper reservoir (Francis et al. 1993). Erebus is a stratovolcano of phonolitic composition that lies in Ross Island, west Antarctica, and hosts a persistent lava lake where large diameter (> 5 m) gas slugs ascend and explosively decompress at the lake’s surface causing strombolian eruptions. VLPs at Erebus are recorded in the near-field (0.7–2.5 km) and constitute a common form of seismic activity (Aster et al. 2003). The waveforms of these VLPs consist of the initial part which exhibits the highest amplitude

and the coda part with a duration of tens of seconds, however, in most cases it is difficult to find the exact time boundary that separates the two parts (Fig. 11). Multiyear observations have revealed that the initial part of VLPs may be quite variable in contrast to the coda part that is very similar among different events through time. Moment tensor inversion of VLPs points to a shallow ( $< 1$  km) source beneath the lava lake that represents a combination of moment tensor and a downward force indicating upward acceleration of melt (Aster et al. 2008).

Figure 11 depicts a physical mechanism of VLPs generation at Erebus as suggested by Knox et al. (2018) based on waveform characteristics, source inversion results and images taken from a time-lapse camera installed near the lava lake. Initially gas bubbles coalesce and form large slugs near the base of the conduit that connects the lake with the deeper reservoir. The gas slug then ascends a seismically through the conduit growing in size due to decompression and bursts near the surface generating the initial part of the VLP waveform. This strombolian eruption removes material from the top part of the lava lake and disturbs the gravitational equilibrium between the lake and the melt that resides inside the conduit. The gradual refilling of melt at the base of the conduit progressively restores the equilibrium and is also responsible for the decaying coda of the VLPs. The variation in explosion styles of the slugs can then explain the variable initial part of VLPs, while the stable conduit geometry gives rise to the very similar coda of VLPs at different time periods. At lava lakes, weak VLPs can be also generated by gas-pistoning which is a term that refers to the cyclic rise and fall of a crusted lava surface (Swanson et al. 1979). Chouet and Dawson (2015) analyzed such VLPs with periods of about 20.5 s and attributed them to a mechanism of foam formation and collapse that results in gas accumulation and loss at the top of the lava column.

Another mechanism of VLP generation in lava lakes has to do with rockfalls that impact the surface of the lake, creating in this way a disturbance that propagates downwards through coupling at the fluid-rock interface. Chouet and Matoza (2013) found numerous VLPs that occurred during episodes of deflation of the Kilauea summit whose locations

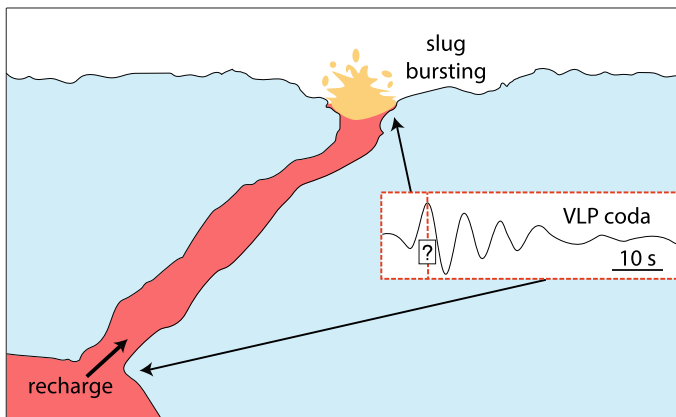


**Fig. 11** Geometrical configuration of the conduit that connects the magma reservoir with the lava lake at Erebus volcano (after Knox et al. 2018). Large gas slugs ascend through the conduit a seismically and burst at the surface of the lake removing material and initiating the oscillatory recharge of the conduit. The initial part of the VLP waveform corresponds to the slug bursting and the coda part to the recharge phase. The question mark denotes the uncertainty in defining when exactly the one phase stops and the other phase starts

were ~1 km below the lava lake that is hosted at the Halemaumau pit crater. These events resembled the VLPs at Erebus, with high initial amplitude followed by a decaying coda coinciding in time with visual observations of rockfalls in the lake. Moment tensor inversion performed using stacked VLP waveforms determined that the source could be adequately represented by time-dependent moment tensor elements without the need to include single forces.

Figure 12a shows the possible configuration of the lava lake, conduit and magma chamber beneath Halemaumau whose equilibrium is disturbed once the rockfalls start occurring. Chouet and Matoza (2013) argued that a simple mechanical analog of this configuration is a body with variable mass  $m(t)$ , representing the amount of melt in the lake, which lies on top of an elastic spring with constant  $k$  that accounts for the compressibility of the melt and the elasticity of the encasing rocks (cf. Fig. 12b). The authors further developed a lumped parameter model that describes the vertical displacement  $z$  of the mass (lava lake surface) when the system is subjected to an external force  $F_e(t)$  (produced by the rockfalls) and the movement is constrained by friction at the walls (damping due to melt viscosity). This leads to a second order differential equation of the form

$$m(t) \frac{d^2 z}{dt^2} + b \frac{dz}{dt} + kz = F_e(t) \quad (14)$$

where  $b$  is the damping coefficient that depends on magma viscosity and the conduit length. The numerical solutions of this equation can be used to estimate volume changes of magma in the system as a function of time such that

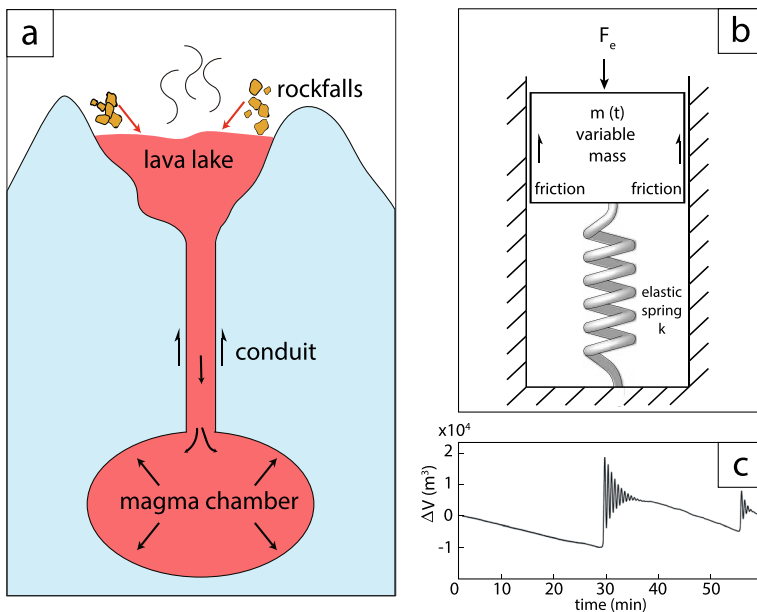


**Fig. 12** **a** The configuration of the lava lake and plumbing system beneath Kilauea volcano. Rockfalls impact the surface of the lava lake and trigger VLPs due to conduit oscillations, **b** simple analog model of the lava lake-conduit-magma chamber system (see text for more details), and **c** changes in volume of the material in the lake as a function of time calculated using a simple, lumped parameter model described in the main text (after Chouet and Dawson 2013)



$$\Delta V(t) = z(t)A_c \quad (15)$$

where  $A_c$  is the conduit cross-section. The best agreement between these volume change estimates and the ones inferred from the time-dependent moment tensor of VLPs can be achieved for rockfall volumes between 200 and 4500 m<sup>3</sup> (cf. Fig. 12c).

It is interesting to note that the physical mechanisms of VLPs generation at lava lakes described above have a ‘top-down’ form (Patrick et al. 2011), in the sense that a superficial disturbance in the lake (degassing, slug bursting, rockfalls) sets into oscillatory motion the plumbing system, producing VLPs with a decaying coda. Liang et al. (2020a, 2020b) utilized this idea and extended the simple oscillation model of Chouet and Matoza (2013) in order to perform a Bayesian inversion of VLP features (oscillation period, decay rates, surface displacement spectra) in order to infer the conduit geometry and viscosity of magma in the Kilauea lava lake. Notable additions to the oscillation model is the inclusion of gravity in the form of magma buoyancy and viscous boundary layers along the conduit walls. The inversion results showed that magma inside the conduit exhibits density stratification which is essential for the generation of VLP oscillations by providing the necessary buoyancy. In the same spirit, Crozier and Karlstrom (2022) utilized features of VLPs that occurred at different time periods in order to study the evolution of magma temperature and volatile content in the years 2008–2018 at Kilauea.

## 5 VLPs in the Era of Machine Learning

In recent years machine learning techniques have become very useful in seismology as a means of detecting seismic signals and patterns within large volumes of data, a task that would otherwise be time consuming and heavily influenced by subjective choices made by the analyst (for an overview see Kong et al. 2019). The two main types of machine learning algorithms are namely supervised and unsupervised learning, where the difference between the two lies in the requirement of the former to first train the algorithm with known data before its application to an unknown dataset. Supervised machine learning is typically used in signal classification problems employing algorithms such as neural networks, support vector machines or random forest, while unsupervised learning is primarily used in clustering data by similarity with algorithms such as K-means, spectral or hierarchical clustering (for more details see Theodoridis and Koutroumbas 2009). Classification of seismic signals into categories and the grouping of each category of signals into families based on their similarity, are both important tasks in the field of volcano seismology. Examples of the application of machine learning algorithms at different volcanoes can be found in Piton de la Fournaise (Maggi et al. 2017), Ubinas in Peru (Malfante et al. 2018), Cotopaxi in Ecuador (Duque et al. 2020) and Redoubt in Alaska (Konstantinou et al. 2022) among others.

The application of machine learning algorithms to VLPs is so far limited to few volcanoes where the quality and quantity of the recorded data is sufficiently high in order to obtain significant results. At Stromboli volcano (Esposito et al. 2008) utilized unsupervised machine learning in the form of Self-Organized Maps in order to obtain families of VLP events and then correlated each family to particular vents that were erupting. More recently, Romano et al. (2022) applied the same machine learning algorithm to VLP data recorded by a strainmeter installed at Stromboli and also found that events can be clustered in two large families. At White Island volcano, Park et al. (2020) used waveform semblance to detect VLP events during 2013–2020 and then employed some of these events as templates



in order to further identify VLPs that occurred prior to 2013 when only one station was available. The authors then applied hierarchical clustering to the combined VLPs catalog and obtained two families of events, one of which was found to systematically occur prior to unrest periods. All of the above studies agree that the similarity of VLP events within a single family may either be due to similar location, and/or due to a similar source process that repeats itself in a non-destructive way. However, as shown by Esposito et al. (2008) location may not always be the most important factor of the two, since VLPs with similar waveforms were located beneath different vents, suggesting that the source time history of these events contributed more to their similarity than source location. At Kilauea Dawson et al. (2010) have utilized a Hidden Markov model of pattern recognition in order to detect VLPs generated due to episodic degassing in the lava lake.

Future applications of machine learning algorithms for the purpose of classifying VLPs by waveform similarity could focus on two possibilities: (1) the analysis of older archived datasets, and (2) the real-time detection of VLPs that may occur prior to unrest or phreato-magmatic activity. At many volcanoes worldwide there is an already accumulated archive of recorded continuous data that can be utilized in order to detect and classify VLPs in different families using the techniques mentioned previously. Each family of VLPs could then be associated with past periods of unrest and eruptions, while stacked waveforms of each family could be located and inverted for deciphering source processes. The stacked waveforms of VLPs that occurred prior to eruptions can also be utilized as a template in order to identify similar VLPs in real-time and thus provide warning before the onset of an eruption. This may be particularly important in the case of VLPs that precede intense phenomena such as phreatic eruptions or caldera collapses.

Another future application of machine learning has to do with analyzing data acquired through the deployment of Distributed Acoustic Sensing (DAS) at volcanic environments. DAS is a promising technological development that measures strain in an optical fiber using interferometry once this fiber becomes slightly deformed due to the disturbance generated by propagating seismic waves. The length of a DAS cable that contains the optical fiber may vary from hundreds of meters to several kilometers and the cable is usually buried within some tens of centimeters beneath the surface. The main advantage of DAS cables over traditional seismometers is that they have a spatial resolution of a few meters, thus providing high spatial as well as temporal density of the recorded seismic wavefield. This high sampling density also entails an enormous volume of acquired data that needs to be analyzed and it is exactly the point where machine learning algorithms can be applied. At active volcanoes pilot studies of DAS cable deployments have already been performed and have shown the potential for DAS to become the standard way of recording and monitoring seismicity at volcanic environments (e.g., Klaasen et al. 2021; Jousset et al. 2022). More specifically, DAS has been shown to reliably record frequencies down to 0.01–0.03 Hz (Klaasen et al. 2021; Shinohara et al. 2022). In this respect it is expected that machine learning will be essential in the analysis of DAS acquired data by recognizing patterns in VLPs as well as in any other volcanoseismic signals.

## 6 Concluding Remarks

It is now widely recognized that volcanoes represent broadband sources of seismic energy and that within the group of volcanoseismic signals VLPs constitute the lowest end member based on their frequency content. This makes VLPs less prone to distorting propagation

effects than other signals and hence they have been considered as good targets for detailed source studies. The fact that VLPs are detected in different volcano types and they can be generated by a variety of physical mechanisms, also contributes towards their potential usefulness in elucidating fluid mass movement beneath active volcanoes. This review has highlighted several methodological issues that could be improved or further investigated in the future in an effort to better constrain source models and their physical interpretation:

- Most unconstrained source inversions of VLPs follow a point-source approximation and focus only on the temporal evolution of the source properties. A fundamental criticism of such an approach is that it completely ignores the spatial extent of the source which is expected to be considerable, since fluids flow within finite dimension conduits. Legrand and Perton (2022) have recently proposed an inversion methodology for VLPs recorded at Stromboli that makes use of a spatially extended conduit in order to recover the fluid overpressure and depth of the magma column beneath the crater surface. It remains to be seen whether an extended source description for VLPs will become more common or even replace point-source approximation in the future. This development would complement the use of extended sources for the analysis of crack resonance in LP events (e.g., Nakano et al. 2007).
- Single forces are commonly included in the source description of VLPs, which appears to be a plausible source component, taking into account the likely vertical acceleration of fluids. However, it has become clear by now that factors such as data quality or source mislocation (aggravated by the dominance of near-field effects in VLP signals) can severely hamper attempts to show that single forces significantly contribute to the overall amplitude of VLPs. One approach to tackle this problem is to perform synthetic tests using a variety of scenarios involving sources with and without single forces, different noise levels, and variable degree of source mislocation. These tests will help to determine to what extent and with what confidence level single forces can be recovered. Higher resolution images of the shallow velocity structure at volcanoes would also help to improve location accuracy of VLPs and minimize the chances of including spurious single forces in their source representation.
- The passband of seismic sensors and the subsequent processing of the recorded seismograms have been found to potentially generate artifacts when the source time function of the VLPs has a ramp-like long duration. This issue has to be further investigated by analyzing different datasets and by quantifying to what extent these artifacts can affect source inversion results. In such cases co-location of GPS receivers and seismometers is beneficial in order to detect artifacts by comparing synthetic (GPS-derived) and recorded seismograms.
- Poisson ratios determined from the eigenvalues of VLP moment tensors were found to be much larger ( $> 0.4$ ) than the value expected for a Poisson solid ( $\sim 0.25$ ), or the value commonly assumed for volcanic environments ( $\sim 0.33$ ). This discrepancy influences the exact relationship of the Lamé parameters, resulting in an increase in the uncertainty of volume change estimated from the seismic moment of VLPs. Caution should then be exercised when interpreting this volume change as the quantity of fluid that has entered or vacated the plumbing system of the volcano under study. Anomalous Poisson ratios are not only observed in the case of VLPs but also in a multitude of other signals (microearthquakes, man-made explosions, cavity collapses) as reported by Tape and Tape (2013). Poor station coverage and limited knowledge of the velocity structure may have played a significant role in some of these cases, however, it is doubtful that they are the sole cause for all of them.

- The study of VLP signals would greatly benefit from a rigorous statistical analysis of their properties (period, source depth, seismic moment and moment tensor, etc) and their comparison among different volcanoes, as attempted in a rudimentary way in this work. This would require detailed catalogs of VLPs being compiled for each volcano that would be publicly available much in the same way that catalogs of volcano-tectonic or LP earthquakes are. This would offer more insight into the source generation of VLPs and further promote open and transparent research in this field.

In terms of instrumentation, new technological developments such as DAS or 6 degrees of freedom seismometers have the potential to steeply increase the quantity and quality of data at active volcanoes, a prospect that will undoubtedly have a large impact on the study of VLPs. The application of efficient machine learning algorithms will then provide valuable new knowledge in the occurrence patterns and source properties of VLPs as well as other volcanoseismic signals.

**Supplementary Information** The online version contains supplementary material available at <https://doi.org/10.1007/s10712-023-09800-0>.

**Acknowledgements** I would like to thank Mrs Venus Chiu for her help in preparing the Figures that appear in this work. I am also grateful to Zacharie Duputel, Ivan Lokmer and an anonymous reviewer for their comments and constructive criticism that improved substantially this work.

**Funding** This work has been financially supported by the Ministry of Science and Technology Of Taiwan (MOST) in the form of a research grant.

**Availability of Data and Materials** All the data that appear in the Figures of this work have been adopted from published papers cited in the text and in the supplementary material.

## Declarations

**Conflict of interest** The author declares no known competing interests that could have appeared to influence the work reported in this paper.

**Open Access** This article is licensed under a Creative Commons Attribution 4.0 International License, which permits use, sharing, adaptation, distribution and reproduction in any medium or format, as long as you give appropriate credit to the original author(s) and the source, provide a link to the Creative Commons licence, and indicate if changes were made. The images or other third party material in this article are included in the article's Creative Commons licence, unless indicated otherwise in a credit line to the material. If material is not included in the article's Creative Commons licence and your intended use is not permitted by statutory regulation or exceeds the permitted use, you will need to obtain permission directly from the copyright holder. To view a copy of this licence, visit <http://creativecommons.org/licenses/by/4.0/>.

## References

- Aki K, Richards PG (2002) Quantitative seismology: theory and methods. University Science Books, Sausalito
- Akaike H (1974) A new look at the statistical model identification. *Trans Auto Contr* AC19, 716–723
- Almendros J, Chouet BA, Dawson P, Bond T (2002) Identifying elements of the plumbing system beneath Kilauea Volcano, Hawaii, from the source location of very long period signals. *Geophys J Int* 148:303–312
- Anderson K, Johanson IA, Patrick MR, Gu M, Seagall P, Poland M, Montgomery-Brown EK, Miklius A (2019) Magma reservoir failure and the onset of caldera collapse at Kilauea volcano in 2018. *Science* 366:1214. <https://doi.org/10.1126/science.aaz1822>
- Aster R, Mah S, McIntosh W, Dunbar N, Johnson J, Ruiz M, McNamara S (2003) Very long period oscillations of Mount Erebus volcano. *J Geophys Res* 108:2522. <https://doi.org/10.1029/2002JB002101>

- Aster R, Zandomenighi D, Mah S, McNamara S, Henderson DB, Knox H, Jones K (2008) Moment tensor of very long period seismic signals from Strombolian eruptions of Erebus volcano. *J Volc Geotherm Res* 177:635–647. <https://doi.org/10.1016/j.volgeores.2008.08.013>
- Auger E, D'Auria L, Martini M, Chouet B, Dawson P (2006) Real-time monitoring and massive inversion of source parameters of very long period seismic signals: an application to Stromboli volcano, Italy. *Geophys Res Lett* 33:L04031. <https://doi.org/10.1029/2005GL024703>
- Bean C, Lokmer I, O'Brien G (2008) Influence of near-surface volcanic structure on long-period seismic signals and on moment tensor inversions: simulated examples from Mount Etna. *J Geophys Res* 113:B08308. <https://doi.org/10.1029/2007JB005468>
- Bean CJ, De Barros L, Lokmer I, Métaixian J-P, O'Brien G, Murphy S (2014) Long-period seismicity in the shallow volcanic edifice formed from slow-rupture earthquakes. *Nat Geosci* 7:71–75. <https://doi.org/10.1038/NGEO2027>
- Cannata A, Hellweg M, Di Grazia G, Ford S, Alparone S, Gresta S, Montalto P, Patane D (2009) Long period and very long period events at Mt Etna volcano: characteristics, variability and causality, and implications for their sources. *J Volc Geotherm Res* 187:227–249. <https://doi.org/10.1016/j.volgeores.2009.09.007>
- Caudron C, Taisne B, Neuberg J, Jolly AD, Christenson B, Lecocq T, Suparjan D, Syahbana G, Suan-tika (2018) Anatomy of phreatic eruptions. *Earth Planets Space* 70:168. <https://doi.org/10.1186/s40623-018-0938-x>
- Cesca S, Letort J, Razafindrakoto HNT, Heimann S, Rivalta E, Isken MP, Nikkhoo M, Passarelli L, Petersen GM, Cotton F, Dahm T (2020) Drainage of a deep magma reservoir near Mayotte inferred from seismicity and deformation. *Nat Geosci* 13:87–93. <https://doi.org/10.1038/s41561-019-0505-5>
- Chouet BA (1996) Long-period volcano seismicity: its source and use in eruption forecasting. *Nature* 380:309–316
- Chouet BA (2003) Volcano seismology. *Pure Appl Geophys* 160:739–788. <https://doi.org/10.1007/PL00012556>
- Chouet B, Dawson P, Ohminato T, Martini M, Saccorotti G, Guidipietro F, De Luca G, Milana G, Scarpa R (2003) Source mechanisms of explosions at Stromboli volcano, Italy, determined from moment-tensor inversions of very-log-period data. *J Geophys Res* 108:2019. <https://doi.org/10.1029/2002JB001919>
- Chouet B, Dawson P, Arciniega-Ceballos A (2005) Source mechanism of vulcanian degassing at Popocatepetl volcano, Mexico, determined from waveform inversions of very long period signals. *J Geophys Res* 110:B07301. <https://doi.org/10.1029/2004JB003524>
- Chouet BA, Dawson PB, James MR, Lane SJ (2010) Seismic source mechanism of degassing bursts at Kilauea volcano, Hawaii: results from waveform inversion in the 10–50 s band. *J Geophys Res* 115:B09311. <https://doi.org/10.1029/2009JB006661>
- Chouet BA, Dawson PB (2011) Shallow conduit system at Kilauea volcano, Hawaii, revealed by seismic signals associated with degassing bursts. *J Geophys Res* 116:B12317. <https://doi.org/10.1029/2011JB008677>
- Chouet BA, Matoza RS (2013) A multi-decadal view of seismic methods for detecting precursors of magma movement and eruption. *J Volc Geotherm Res* 252:108–175. <https://doi.org/10.1016/j.volgeores.2012.11.013>
- Chouet BA, Dawson PB (2013) Very long period conduit oscillations induced by rockfalls at Kilauea volcano, Hawaii. *J Geophys Res* 118:5352–5371. <https://doi.org/10.1002/jgrb.50376>
- Chouet BA, Dawson PB (2015) Seismic source dynamics of gas-piston activity at Kilauea volcano, Hawaii. *J Geophys Res Solid Earth* 120:2525–2560. <https://doi.org/10.1002/2014JB011789>
- Chouet BA, Dawson PB (2016) Origin of the pulse-like signature of shallow long-period volcano seismicity. *J Geophys Res Solid Earth* 121. <https://doi.org/10.1002/2016JB013152>
- Crozier J, Karlstrom L (2022) Evolving magma temperature and volatile contents over the 2008–2018 summit eruption of Kilauea Volcano. *Sci Adv* 8:eabm4310. <https://doi.org/10.1126/sciadv.abm4310>
- Dawson P, Whilldin D, Chouet B (2004) Application of near real-time radial semblance to locate the shallow magmatic conduit at Kilauea Volcano, Hawaii. *Geophys Res Lett* 31:L21606. <https://doi.org/10.1029/2004GL021163>
- Dawson PB, Benítez MC, Chouet BA, Wilson D, Okubo PG (2010) Monitoring very-long-period seismicity at Kilauea Volcano, Hawaii. *Geophys Res Lett* 37:L18306. <https://doi.org/10.1029/2010GL044418>
- Dawson P, Chouet B (2014) Characterization of very-long-period seismicity accompanying summit activity at Kilauea Volcano, Hawaii: 2007–2013. *J Volc Geotherm Res* 278–279. <https://doi.org/10.1016/j.volgeores.2014.04.010>

- Davi R, O'Brien GS, Lokmer I, Bean CJ, Lesage P, Mora MM (2010) Moment tensor inversion of explosive long period events recorded on Arenal volcano, Costa Rica, constrained by synthetic tests. *J Volc Geotherm Res* 194:189–200. <https://doi.org/10.1016/j.jvolgeores.2010.05.012>
- De Barros L, Lokmer I, Bean CJ (2013) Origin of spurious single forces in the source mechanism of volcanic seismicity. *J Volc Geotherm Res* 262:1–6. <https://doi.org/10.1016/j.jvolgeores.2013.06.006>
- Duputel Z, Rivera L (2019) The 2007 caldera collapse of Piton de la Fournaise volcano: source process from very-long-period seismic signals. *Earth Planet Sci Lett* 527:115786. <https://doi.org/10.1016/j.epsl.2019.115786>
- Duputel Z, Lengliné O, Ferrazzini V (2019) Constraining spatiotemporal characteristics of magma migration at Piton De La Fournaise Volcano from pre-eruptive seismicity. *Geophys Res Lett* 46:119–127. <https://doi.org/10.1029/2018GL080895>
- Duque A, Gonzalez K, Perez N, Benitez D, Grijalva F, Lara-Cueva R, Ruiz M (2020) Exploring the unsupervised classification of seismic events of Cotopaxi volcano. *J Volc Geotherm Res* 403:107009. <https://doi.org/10.1016/j.jvolgeores.2020.107009>
- Esposito AM, Giudiciopietro F, D'Auria L, Scarpetta S, Martini MG, Coltelli M, Marinaro M (2008) Unsupervised neural analysis of Very-Long-Period events at Stromboli volcano using the self-organizing maps. *Bull Seismol Soc Am* 98:2449–2459. <https://doi.org/10.1785/0120070110>
- Eyre T, Bean CJ, De Barros L, Martini F, Lokmer I, Mora MM, Pacheco JF, Soto GJ (2015) A brittle failure model for long-period seismic events recorded at Turrialba volcano, Costa Rica. *J Geophys Res Solid Earth* 120:1452–1472. <https://doi.org/10.1002/2014JB011108>
- Ferrazzini V, Aki K (1987) Slow waves trapped in a fluid-filled infinite crack: implication for volcanic tremor. *J Geophys Res* 92:9215–9223
- Flinders AF, Johanson IA, Dawson PB, Anderson KR, Haney MM, Shiro MM (2020) Very-Long-Period (VLP) seismic artifacts during the 2018 caldera collapse at Kilauea, Hawaii. *Seismol Res Lett* 91:3417–3432. <https://doi.org/10.1785/0220200083>
- Fontaine FR, Roult G, Hejrani B, Michon L, Ferrazzini V, Barruol G, Talcic H, Di Muro A, Peltier A, Raymond D, Staudacher T, Massin F (2019) Very- and Ultra-long-period seismic signals prior to and during caldera formation on La Reunion island. *Sci Rep* 9:8068. <https://doi.org/10.1038/s41598-019-44439-1>
- Francis P, Oppenheimer C, Stevenson D (1993) Endogeneous growth of persistently active volcanoes. *Nature* 366:554–557. <https://doi.org/10.1038/366554a0>
- Gercek H (2007) Poisson's ratio values for rocks. *Int J Rock Mech Min Sci* 44:1–13
- Gerst A, Savage MK (2002) Seismic anisotropy beneath Ruapehu volcano: a possible eruption forecasting tool. *Science* 306:1543–1547. <https://doi.org/10.1126/science.1103445>
- Gudmundsson A (2015) Collapse-driven large eruptions. *J Volc Geotherm Res* 304:1–10. <https://doi.org/10.1016/j.jvolgeores.2015.07.033>
- Gudmundsson MT, Jónsdóttir K, Hooper A, Holohan EP, Halldórsson SA, Ófeigsson BG, Cesca S, Vogfjörð KS, Sigmundsson F, Högnadóttir T, Einarsson P (2016) Gradual caldera collapse at Bárðarbunga volcano, Iceland, regulated by lateral magma outflow. *Science* 353:aaf8988. <https://doi.org/10.1126/science.aaf8988>
- Guidiciopietro F, D'Auria L, Martini M, Caputo T, Peluso R, De Cesare W, Orazi M, Scarpato G (2009) Changes in the VLP seismic source during the 2007 Stromboli eruption. *J Volc Geotherm Res* 182:162–171. <https://doi.org/10.1016/j.jvolgeores.2008.11.008>
- Haney MM, Chouet BA, Dawson PB, Power JA (2013) Source characterization for an explosion during the 2009 eruption of Redoubt volcano from very-long-period waves. *J Volc Geotherm Res* 259:77–88. <https://doi.org/10.1016/j.jvolgeores.2012.04.018>
- Harrington RM, Brodsky EE (2007) Volcanic hybrid earthquakes that are brittle-failure events. *Geophys Res Lett* 34:L06308. <https://doi.org/10.1029/2006GL028714>
- Hendriyana A, Tsuji T (2019) Migration of very long period seismicity at Aso volcano, Japan, associated with the 2016 Kumamoto earthquake. *Geophys Res Lett* 46:8763–8771. <https://doi.org/10.1029/2019GL082645>
- Hidayat D, Voight B, Langston C, Ratdomopurbo A, Ebeling C (2000) Broadband seismic experiment at Merapi volcano, Java, Indonesia: very-long-period pulses embedded in multiphase earthquakes. *J Volc Geotherm Res* 100:215–231
- Hidayat D, Chouet B, Voight B, Dawson P, Ratdomopurbo A (2002) Source mechanism of very-long-period signals accompanying dome growth activity at Merapi volcano, Indonesia. *Geophys Res Lett* 29:2118. <https://doi.org/10.1029/2002GL015013>
- Hill DP, Dawson P, Johnston MJS, Pitt AM, Biasi G, Smith K (2002) Very-long-period volcanic earthquakes beneath Mammoth Mountain, California. *Geophys Res Lett* 29:1370. <https://doi.org/10.1029/2002GL014833>

- James MR, Lane SJ, Chouet BA, Gilbert JS (2004) Pressure changes associated with the ascent and bursting of gas slugs in liquid-filled vertical and inclined conduits. *J Volc Geotherm Res* 129:61–82
- James MR, Lane SJ, Chouet BA (2006) Gas slug ascent through changes in conduit diameter: laboratory insights into a volcano-seismic source process in low-viscosity magmas. *J Geophys Res* 111:B05201. <https://doi.org/10.1029/2005JB003718>
- Jolly AD, Lokmer I, Thun J, Salichon J, Fry B, Chardot L (2017) Insights into fluid transport mechanisms at White island from analysis of coupled very long-period (VLP), long-period (LP) and high-frequency (HF) earthquakes. *J Volc Geotherm Res* 343:75–94. <https://doi.org/10.1016/j.jvolgeores.2017.06.006>
- Jousset P, Budi-Santoso A, Jolly AD, Boichu M, Surono S, Dwiyono S, Sumarti P, Thierry (2013) Signs of magma ascent in LP and VLP seismic events and link to degassing: an example from the 2010 explosive eruption at Merapi volcano, Indonesia. *J Volc Geotherm Res* 261:171–192. <https://doi.org/10.1016/j.jvolgeores.2013.03.014>
- Jousset P, Currenti G, Schwarz B, Chalari A, Tilmann F, Reinsch T, Zuccarello L, Privitera E, Krawczyk CM (2022) Fibre optic distributed acoustic sensing of volcanic events. *Nat Commun* 13:1753. <https://doi.org/10.1038/s41467-022-29184>
- Kaneshima S, Kawakatsu H, Matsubayashi H, Sudo Y, Tsutsui T, Ohminato T, Ito H, Uhira K, Yamasato H, Oikawa J, Takeo M (1996) Mechanism of phreatic eruptions at Aso volcano inferred from near-field broadband seismic observations. *Science* 273:642–645
- Kawakatsu H, Ohminato T, Ito H (1994) 10s-period volcanic tremors observed over a wide area in southwestern Japan. *Geophys Res Lett* 21:1963–1966
- Kawakatsu H, Kaneshima S, Matsubayashi H, Ohminato T, Sudo Y, Tsutsui T, Uhira K, Yamasato H, Ito H, Legrand D (2000) Aso94: Aso seismic observation with broadband instruments. *J Volc Geotherm Res* 101:129–154
- Kazahaya R, Mori T, Takeo M, Ohminato T, Urabe T, Maeta Y (2011) Relations between single very-long-period pulses and volcanic gas emissions at Mt Asama, Japan. *Geophys Res Lett* 38:L11307. <https://doi.org/10.1029/2011GL047555>
- Kazahaya R, Maeda Y, Mori T, Shinohara H, Takeo M (2015) Changes to the volcanic outgassing mechanism from 2007 to 2011 at Mt Asama, Japan, Earth Planet. Sci Lett 418:1–10. <https://doi.org/10.1016/j.epsl.2015.02.034>
- Kilburn CRJ (2003) Multiscale fracturing as a key to forecasting volcanic eruptions. *J Volcanol Geotherm Res* 125:271–289. [https://doi.org/10.1016/S0377-0273\(03\)00117-3](https://doi.org/10.1016/S0377-0273(03)00117-3)
- Kilburn CRJ, Voight B (1998) Slow rock fracture as eruption precursor at Soufriere Hills volcano, Montserrat. *Geophys Res Lett* 29:3665–3668. <https://doi.org/10.1029/98GL01609>
- Klaasen S, Paitz P, Lindner N, Dettmer J, Fichtner A (2021) Distributed acoustic sensing in volcano-glacial environments - Mount Meager, British Columbia. *J Geophys Res Solid Earth* 126:e2021JB022358. <https://doi.org/10.1029/2021JB022358>
- Knox HA, Chaput JA, Aster RC, Kyle PR (2018) Multiyear shallow conduit changes observed with lava lake eruption seismograms at Erebus volcano, Antarctica. *J Geophys Res Solid Earth* 123:3178–3196. <https://doi.org/10.1002/2017JB015045>
- Kobayashi T, Ohminato T, Ida Y, Fujita E (2012) Intermittent inflations recorded by broadband seismometers prior to caldera formation at Miyake-jima volcano in 2000, Earth Planet. Sci Lett 357–358:145–151. <https://doi.org/10.1016/j.epsl.2012.09.039>
- Kong Q, Trugman DT, Ross ZE, Bianco MJ, Meade BJ, Gerstoft P (2019) Machine learning in seismology: turning data into insights. *Seismol Res Lett* 90:3–14. <https://doi.org/10.1785/0220180259>
- Konstantinou KI, Schlindwein V (2003) Nature, wavefield properties and source mechanism of volcanic tremor: a review. *J Volc Geotherm Res* 119:161–187
- Konstantinou KI, Ayu Rahmalia D, Nurfitriana I, Ichihara M (2022) Fast identification of volcanic tremor and lahar signals during the 2009 Redoubt eruption using permutation entropy and supervised machine learning. *Seismol Res Lett* 93:435–443. <https://doi.org/10.1785/0220210176>
- Kumagai H, Chouet BA (2000) Acoustic properties of a crack containing magmatic or hydrothermal fluids. *J Geophys Res* 105:25493–25512
- Kumagai H, Ohminato T, Nakano M, Ooi M, Kubo A, Inoue H, Oikawa J (2001) Very-long-period seismic signals and caldera formation at Miyake island, Japan. *Science* 293:687–689
- Kumagai H, Miyakawa K, Negishi H, Inoue H, Obara K, Suetsugu D (2003) Magmatic dike resonances inferred from Very-Long-Period seismic signals. *Science*. <https://doi.org/10.1126/science.1081195>
- Kumagai H, Chouet BA, Dawson PB (2005) Source process of a long-period event at Kilauea volcano, Hawaii. *Geophys J Int* 161:243–254. <https://doi.org/10.1111/j.1365-246X.2005.02502.x>
- Legrand D, Kaneshima S, Kawakatsu H (2000) Moment tensor analysis of near-field broadband waveforms observed at Aso volcano, Japan. *J Volc Geotherm Res* 101:155–169



- Legrand D, Perton M (2022) What are VLP signals at Stromboli volcano? *J Volc Geotherm Res* 421:107438. <https://doi.org/10.1016/j.jvolgeores.2021.107438>
- Liang C, Karlstrom L, Duhnam EM (2020a) Magma oscillations in a conduit-reservoir system, application to Very-Long-Period (VLP) seismicity at basaltic volcanoes: 1. Theory. *J Geophys Res Solid Earth*, 125:e2019JB017437. <https://doi.org/10.1029/2019JB017437>
- Liang C, Crozier J, Karlstrom L, Duhnam EM (2020b) Magma oscillations in a conduit-reservoir system, application to Very-Long-Period (VLP) seismicity at basaltic volcanoes: 2. Data inversion and interpretation at Kilauea volcano. *J Geophys Res Solid Earth*, 125:e2019JB017456. <https://doi.org/10.1029/2019JB017456>
- Lokmer I, Bean CJ (2010) Properties of the near-field term and its effect on polarisation analysis and source locations of long-period (LP) and very-long-period (VLP) seismic events at volcanoes. *J Volc Geotherm Res* 192:35–47. <https://doi.org/10.1016/j.jvolgeores.2010.02.008>
- Longo A, Papale P, Vassalli M, Saccorotti G, Montagna CP, Cassioli A, Guidice S, Boschi E (2012) Magma convection and mixing dynamics as a source of Ultra Long Period oscillations. *Bull Volcanol* 74:873–880. <https://doi.org/10.1007/s00445-011-0570-0>
- Lyons JL, Waite GP (2011) Dynamics of explosive volcanism at Fuego volcano imaged with very long period seismicity. *J Geophys Res* 116:B09303. <https://doi.org/10.1029/2011JB008521>
- Lyons JL, Waite GP, Ichihara M, Lees J (2012) Tilt prior to explosions and the effect of topography on ultra-long-period seismic records at Fuego volcano, Guatemala. *Geophys Res Lett* 39:L08305
- Maeda Y, Takeo M (2011) Very-long-period pulses at Asama volcano, central Japan, inferred from dense seismic observations. *Geophys J Int* 185:265–282. <https://doi.org/10.1111/j.1365-246X.2011.04938.x>
- Maeda Y, Kato A, Terakawa T, Yamanaka Y, Horikawa S, Matsushiro K, Okuda T (2015a) Source mechanism of a VLP event immediately before the 2014 eruption of Mt Ontake, Japan. *Earth Planets Space* 67:187. <https://doi.org/10.1186/s40623-015-0358-0>
- Maeda Y, Kumagai H, Laason R Jr, Figueroa MS II, Yamashina T, Ohkura T, Baloloy A (2015b) A phreatic explosion model inferred from a very long period seismic event at Mayon volcano, Philippines. *J Geophys Res Solid Earth* 120:226–242. <https://doi.org/10.1002/2014JB011440>
- Maeda Y, Takeo M, Kazahaya R (2019) Comparison of high and low-frequency signal sources for very-long-period seismic events at Asama volcano, Japan. *Geophys J Int* 217:389–404
- Maggi A, Ferrazzini V, Hibert C, Beauducel F, Boissier P, Amemotou A (2017) Implementation of a multistation approach for automated event classification at Piton de la Fournaise volcano. *Seismol Res Lett* 88(3):878–891. <https://doi.org/10.1785/0220160189>
- Malfante M, Dalla Mura M, Metaxian J-P, Mars JJ, Macedo O, Inza A (2018) Machine learning for volcano-seismic signals. *IEEE Signal Process Mag* 1053–5888. <https://doi.org/10.1109/MSP.2017.2779166>
- Matoza RS, Chouet BA, Jolly BA, Dawson PB, Fitzgerald RH, Kennedy BM, Fee D, Iezzi AM, Kilgour GN, Garaebiti E, Cevuar S (2022) High-rate very-long-period seismicity at Yasur volcano, Vanuatu: source mechanism and decoupling from surficial explosions and infrasound. *Geophys J Int* 230:392–426. <https://doi.org/10.1093/gji/ggab533>
- Mavko G, Mukerji T, Dvorkin J (2009) The rock physics handbook. Cambridge University Press, Cambridge
- McKee KF, Roman DC, Waite GP, Fee D (2022) Silent Very Long Period Seismic events (VLPs) at Stromboli volcano, Italy. *Geophys Res Lett* 49:e2022GL100735. <https://doi.org/10.1029/2022GL100735>
- Molina I, Kumagai H, Garcia-Aristizabal A, Nakano M, Moathes P (2008) Source process of very-long-period events accompanying long-period signals at Cotopaxi volcano, Ecuador. *J Volc Geotherm Res* 176:119–133. <https://doi.org/10.1016/j.volgeores.2007.07.019>
- Müller G (2001) Volume change of seismic sources from moment tensors. *Bull Seismol Soc Am* 91:880–884
- Munekane H, Oikawa J, Kobayashi T (2016) Mechanisms of step-like tilt changes and very long period seismic signals during the 2000 Miyakejima eruption: insights from kinematic GPS. *J Geophys Res Solid Earth* 121:2932–2946. <https://doi.org/10.1002/2016JB012795>
- Murase T, McBirney A (1973) Properties of some common igneous rocks and their melts at high temperatures. *GSA Bull* 84:3563–3592
- Nakamichi H, Kumagai H, Nakano M, Okubo M, Kimata F, Ito Y, Obara K (2009) Source mechanism of very-long-period event at Mt Ontake, central Japan: response of the hydrothermal system to magma intrusion beneath the summit. *J Volc Geotherm Res* 187:167–177. <https://doi.org/10.1016/j.volgeores.2009.09.006>
- Nakano M, Kumagai H, Chouet B, Dawson P (2007) Waveform inversion of volcano-seismic signals for an extended source. *J Geophys Res* 112:B02306. <https://doi.org/10.1029/2006JB004490>
- Neal et al (2019) The 2018 rift eruption and summit collapse of Kilauea volcano. *Science* 363:367–374. <https://doi.org/10.1126/science.aav/7046>

- Nishimura T, Nakamichi H, Tanaka S, Sato M, Kobayashi T, Ueki S, Hamaguchi H, Ohtake M, Sato H (2000) Source process of very long period seismic events associated with the 1998 activity of Iwate volcano, northeastern Japan. *J Geophys Res* 105:19135–19147
- Niu J, Song T-RA (2021a) Episodic transport of discrete magma batches beneath Aso volcano. *Nat Commun* 12:5555. <https://doi.org/10.1038/s41467-021-25883-y>
- Niu J, Song T-RA (2021b) The response of repetitive very-long-period seismic signals at Aso volcano to periodic loading. *Geophys Res Lett*, 48:e2021GL092728. <https://doi.org/10.1029/2021GL092728>
- O'Brien GS, Bean CJ (2008) Seismicity on volcanoes generated by slug ascent. *Geophys Res Lett* 35:L16308. <https://doi.org/10.1029/2008GL035001>
- O'Brien GS, Lokmer I, Bean CJ (2010) Statistical selection of the “best” seismic source mechanisms from inversions of synthetic volcanic long-period events. *J Geophys Res* 115:B09303. <https://doi.org/10.1029/2009JB006958>
- Ohminato T, Chouet BA, Dawson P, Kedar S (1998) Waveform inversion of very long period impulsive signals associated with magmatic injection beneath Kilauea volcano, Hawaii. *J Geophys Res* 103:23839–23862
- Ohminato T (2006) Characteristics and source modeling of broadband seismic signals associated with the hydrothermal system at Satsuma-Iwojima volcano, Japan. *J Volc Geotherm Res* 158:467–490. <https://doi.org/10.1016/j.volgeores.2006.08.004>
- Park I, Jolly A, Lokmer I, Kennedy B (2020) Classification of long-term very long period (VLP) volcanic earthquakes at Whakaari/White island volcano, New Zealand. *Earth Planets Space* 72:92. <https://doi.org/10.1186/s40623-020-01224-z>
- Patrick M, Wilson D, Fee D, Orr T, Swanson D (2011) Shallow degassing events as a trigger for very-long-period seismicity at Kilauea volcano, Hawaii. *Bull Volcanol* 73:1179–1186. <https://doi.org/10.1007/s00445-011-0475-y>
- Ripepe M, Delle Donne D, Legrand D, Valade S, Lacanna G (2021) Magma pressure discharge induces very long period seismicity. *Sci Rep* 11:20065. <https://doi.org/10.1038/s41598-021-99513-4>
- Rodgers PW (1968) The response of the horizontal pendulum seismometer to Rayleigh and Love waves, tilt, and free oscillations of the Earth. *Bull Seismol Soc Am* 58:1384–1406
- Romano P, Di Lieto B, Scarpetta S, Apicella I, Linde AT, Scarpa R (2022) Dynamic strain anomalies detection at Stromboli before 2019 Vulcanian explosions using machine learning. *Front Earth Sci* 10:862086. <https://doi.org/10.3389/feart.2022.862086>
- Roman D, Cashman KV (2006) The origin of volcano-tectonic swarms. *Geology* 34:457–460. <https://doi.org/10.1130/G22269.1>
- Rowley P, Benson PM, Bean CJ (2021) Deformation-controlled long-period seismicity in low-cohesion volcanic sediments. *Nature Geosci* 14:942–948. <https://doi.org/10.1038/s41561-021-00844-8>
- Segall P, Anderson KR, Johanson I, Miklius A (2019) Mechanics of inflationary deformation during caldera collapse: Evidence from the 2018 Kilauea eruption. *Geophys Res Lett* 46:11782–11789. <https://doi.org/10.1029/2019GL084689>
- Shinohara M, Yamada T, Akuhara T, Mochizuki K, Sakai S (2022) Performance of Seismic Observation by Distributed Acoustic Sensing Technology Using a Seafloor Cable Off Sanriku, Japan. *Front Mar Sci* 9:844506. <https://doi.org/10.3389/fmars.2022.844506>
- Šindijia D, Neuberg J, Smith P (2021) The complex, static displacement of a very long period seismic signal observed at Soufriere Hills volcano, Montserrat, WI. *J Volc Geotherm Res* 413:107209. <https://doi.org/10.1016/j.volgeores.2021.107209>
- Stix J, Maarten de Moor J (2018) Understanding and forecasting phreatic eruptions driven by magmatic degassing. *Earth Planets Space* 70:83. <https://doi.org/10.1186/s40623-018-0855-z>
- Swanson DA, Duffield WA, Jackson DB, Peterson DW (1979) Chronological narrative of the 1969–71 Mauna Ulu eruption of Kilauea Volcano. Hawaii, U.S. Geol. Surv. Prof. Pap., p 1056
- Takei Y, Kumazawa M (1994) Why have the single force and torque been excluded from seismic source models? *Geophys J Int* 118:20–30
- Tape W, Tape C (2013) The classical model for moment tensors. *Geophys J Int* 195:1701–1720. <https://doi.org/10.1093/gji/ggt302>
- Theodoridis S, Koutroumbas K (2009) Pattern recognition. Academic Press, Oxford, UK
- Trovato C, Lokmer I, De Martin F, Aochi H (2016) Long period (LP) events on Mt Etna volcano (Italy): the influence of velocity structures on moment tensor inversion. *Geophys J Int* 207:785–810. <https://doi.org/10.1093/gji/ggw285>
- van Driel M, Wassermann J, Fernanda Nader M, Schubert BSA, Igel H (2012) Strain rotation coupling and its implications on the measurement of rotational ground motions. *J Seismol* 16:657–668. <https://doi.org/10.1007/s10950-012-9296-5>



- van Driel M, Wassermann J, Pelties C, Schiemenz A, Igel H (2015) Tilt effects on moment tensor inversion in the near field of active volcanoes. *Geophys J Int* 202:1711–1721. <https://doi.org/10.1093/gji/ggv209>
- Wassermann J, Braun T, Ripepe M, Bernauer F, Guattari F, Igel H (2022) The use of 6DOF measurement in volcano seismology - A first application to Stromboli volcano. *J. Volc. Geotherm. Res.* 424:107499. <https://doi.org/10.1016/j.jvolgeores.2022.107499>
- Waite GP, Chouet BA, Dawson PB (2008) Eruption dynamics at Mount St Helens imaged from broadband seismic waveforms: interaction of the shallow magmatic and hydrothermal systems. *J Geophys Res* 113:B02305. <https://doi.org/10.1029/2007JB005259>
- Waite GP, Nadeau PA, Lyons JL (2013) Variability in eruption style and associated very long period events at Fuego volcano, Guatemala. *J Geophys Res* 118:1–8. <https://doi.org/10.1002/jgrb.50075>
- Waite GP, Lanza F (2016) Nonlinear inversion of tilt-affected very long period records of explosive eruptions at Fuego volcano. *J Geophys Res Solid Earth* 121. <https://doi.org/10.1002/2016JB013287>
- White RA, McCausland W (2019) A process-based model of pre-eruption seismicity patterns and its use for eruption forecasting at dormant stratovolcanoes. *J Volc Geotherm Res* 382:267–297. <https://doi.org/10.1016/j.jvolgeores.2019.03.004>
- Wielandt E, Forbriger T (1999) Near-field seismic displacement and tilt associated with explosive activity of Stromboli. *Ann Geophys* 42:407–416
- Yamamoto M, Kawakatsu H, Yomogida K, Koyama J (2002) Long-period (12 s) volcanic tremor observed at Usu 2000 eruption: seismological detection of a deep magma plumbing system. *Geophys Res Lett* 29:1329. <https://doi.org/10.1029/2001GL013996>
- Zuccarello L, Burton MR, Saccorotti G, Bean CJ, Patane D (2013) The coupling between very long period seismic events, volcanic tremor, and degassing rates at Mt Etna volcano. *J Geophys Res* 118:4910–4921. <https://doi.org/10.1002/jgrb.50363>

**Publisher's Note** Springer Nature remains neutral with regard to jurisdictional claims in published maps and institutional affiliations.